Science of the Total Environment 619–620 (2018) 988–1002

Contents lists available at ScienceDirect

Science of the Total Environment

journal homepage: www.elsevier.com/locate/scitotenv

Wildfire smoke plumes transport under a subsidence inversion: Climate and health implications in a distant urban area

Elisabeth Alonso-Blanco [a], Amaya Castro [b], Ana I. Calvo [b], Veronique Pont [c], Marc Mallet [c], Roberto Fraile [b,*]

[a] Centre for Energy, Environment and Technology Research (CIEMAT), Department of the Environment, 28040 Madrid, Spain
[b] Department of Physics (IMARENAB), University of León, 24071 León, Spain
[c] Laboratoire d'Aérologie/OMP, UMR 5560, Université de Toulouse III, CNRS-UPS, 14, av. E. Belin, 31400 Toulouse, France

HIGHLIGHTS

- A thermal inversion pushed smoke plume 70 km away from wildfire.
- The air quality in a city 70 km from the forest fire was seriously affected.
- A significant loss of visibility and ashes deposition were observed in the city.
- The radiative forcing estimated in the city indicated strong aerosol absorption.
- Over 40 μg m^{-3} of PM reached the alveolar area of the population in the city.

GRAPHICAL ABSTRACT

ARTICLE INFO

Article history:
Received 20 July 2017
Received in revised form 12 November 2017
Accepted 13 November 2017
Available online xxxx

Editor: P. Kassomenos

Keywords:
Aerosol size distributions
Direct radiative forcing
Respirable fraction
Subsidence inversion
Wildfire

ABSTRACT

This study shows the influence of two large wildfires (one of which was the largest wildfire ever recorded in the region of Castilla y León) in the north-west of the Iberian Peninsula upon the atmospheric air quality of the city of León, Spain, at approximately 70 km from the fires, on days with a strong subsidence inversion associated with high pressures. The vertical dispersion of the smoke plume was inhibited and this caused an increase in the particulate matter (PM) in the atmosphere. During this event, average values of up to 1700 ± 600 particles cm^{-3} were registered, most of which corresponding to the smallest fraction of the fine mode. On the other hand, the count median diameter of the fine mode (CMD_f) increased gradually from 0.09 to 0.14 μm. The PM_{10} and $PM_{2.5}$ reached hourly values of 89 and 36 μg m^{-3}, respectively. This study also estimates the changes in the optical properties of the particles as well as the associated radiative forcing. The presence of an important load of absorbing aerosols was detected, with instantaneous radiative atmospheric forcing up to +134.6 W m^{-2}. The estimations of the respirable fractions showed in healthy adults high levels of mass concentration of the aerosol that reaches the bronchioles and alveoli (up to 43 μg m^{-3}).

1. Introduction

Aerosols from biomass burning are by far the main type of aerosol produced by combustion processes (IPCC, 2001, 2013). Many studies have focused on this field, since biomass burning events do not only alter the properties of atmospheric particulate matter (physical, chemical and optical properties) (Reid et al., 2004; Reid et al., 2005), but also

Abbreviations: b_{scat}, b_{abs}, b_{ext} and b_{bscat}, coefficients of scattering, absorption, extinction and backscattering, respectively; CMD, count median diameter; EC, elemental carbon; MSE, MAE, MEE and MBSE, mass efficiencies of scattering, absorption, extinction and backscattering, respectively; OC, organic carbon; PCASP, passive cavity aerosol spectrometer probe; PM, particulate matter; RI, refractive index; SMD, surface mean diameter; VMD, volume mean diameter.

* Corresponding author.
E-mail address: roberto.fraile@unileon.es (R. Fraile).

https://doi.org/10.1016/j.scitotenv.2017.11.142
0048-9697/

trigger important changes in the concentrations of different atmospheric gases (Adler et al., 2011).

Wildfires significantly increase the concentration of particles corresponding mainly to the submicrometric fraction (Reid et al., 2005), and, consequently, change the aerosol size and mass distribution. Likewise, the concentrations of gases such as CO_2, CO, CH_4, NO_x ($NO + NO_2$) and SO_2 also increase (Andreae and Merlet, 2001; Kasischke and Bruhwiler, 2002). Factors such as the type of fuel, the availability of oxygen and the temperature (Scholes et al., 1996), and also the combustion phase of the wildfire (flaming or smoldering) determine the efficiency of the combustion process. During the flaming phase the concentration of particles released is higher and the particles are smaller (Levine, 1996; Yamasoe et al., 2000) than in the smoldering phase. In addition, gases such as NO_2 and SO_2 are produced at high temperatures which are only reached during the flaming phase and when the forest fuel is totally burned (Sinha et al., 2003).

The aerosols released by these sources are mainly formed by organic matter (Carrico et al., 2005), especially elemental carbon (EC) and primary organic carbon (OC) (Duan et al., 2004; IPCC, 2001). Smaller amounts of other compounds are also found, including nitrate, ammonia and sulphur. The latter, which form the inorganic fraction of the aerosol, are determined by the characteristics of the fuel during the burning process (Andreae and Merlet, 2001) and in the combustion phase (Alves et al., 2010; Yamasoe et al., 2000). The amount of these ionic compounds conditions the hygroscopic properties of this type of aerosol (Carrico et al., 2005). An increase in the soot concentration implies a decrease in the hygroscopicity of the particles released (Rissler et al., 2006).

Besides, the generation of aerosols during wildfires entails significant variations in the energetic balance (IPCC, 2013), which affects the climate. The aerosols from biomass burning may have either a warming or a cooling effect on climate as the optical properties of smoke depend on the geographical source region, the season and the type of biomass burning (Carslaw et al., 2010; Forster et al., 2007). Direct radiative forcings of smoke aerosols have been widely documented to improve our knowledge of the impact on atmospheric dynamics and thermodynamics (semi direct effect). The significant decrease of solar energy at the surface may strongly modify the surface energy budget (Toll et al., 2015). Latent heat and sensible heat fluxes from the surface are consequently disturbed, as shown in Pere et al. (2011). The reduction in surface latent and sensible heat fluxes associated with biomass burning impact could reduce cloudiness (Jiang and Feingold, 2006). In other circumstances, smoke aerosols overlaying bright clouds could increase buoyancy in low layers, thus inhibiting the entrainment of dry air through the cloud-top, thereby helping to preserve humidity and cloud cover in the boundary layer (Wilcox, 2010).

Furthermore, during wildfire events the local meteorological conditions, mainly thermal inversions, and the wind direction, determine the land area affected by the pollution (Duan et al., 2004). The characteristics of the aerosols from biomass burning and the gases released cause a significant deterioration in air quality, with the subsequent impact on human health (Pope, 2000) and visibility (Badarinath et al., 2004). The size/surface relation of the particles, together with their composition and aging, determine their capacity for entering the respiratory system (Oberdärster et al., 2005). In addition, the hygroscopic capacity influences the deposition pattern. Löndahl et al. (2009) observed that the growth of the particles from biomass burning increases the likelihood of deposition in the respiratory tract.

In Spain, most wildfires occur in summer, especially in the northwest. The aim of the present study is to analyze the influence of two large wildfires (burnt area > 500 ha) upon the atmospheric air in the city of León (Spain), 70 km away from the wildfires. Furthermore, one of the wildfires was the largest one ever recorded in the region of Castilla y León. The changes in the physical and optical properties of the aerosols have been analyzed considering specific properties of the burnt vegetal species, as well as the associated shortwave direct radiative forcing. In addition, the changes in the air quality registered in the city of León have been studied in detail, together with the immediate consequences on human health, which have been assessed by estimating the respirable and tracheobronchial mass fractions. The relevance of this study lies in the particular meteorological situation during some of the days in which the wildfires were registered. A strong subsidence inversion inhibited the vertical dispersion of the smoke plumes, considerably deteriorating the air quality.

2. Measurement site

The sampling was carried out in the city of León, Spain, in the northwest of the Iberian Peninsula: 42° 35′ 56″ N 05° 34′ 01″ W. The city center is located at an altitude of 837 m ASL on the fluvial terrace formed by the rivers Bernesga and Torio. The municipality of León covers an area of 39.03 km^2 and the population density is 3401.08 inhabitans/km^2.

The wildfire in Cubo de Benavente (42° 07′ 25″ N, 06° 09′ 47″ W) and the wildfire in Castrocontrigo (42° 10′ 58″ N, 6° 11′ 18″ W) were both detected in the city of León by the end of August 2012.

According to the data from the Spanish Meteorogical Agency (AEMET, in its Spanish acronym) and gathered at the airport of León, located in La Virgen del Camino (42° 35′ 18″ N, 5° 39′ 4″ W), at 5.1 km from the city center, the climate of León is a continentalized Mediterranean climate mitigated by the closeness of the Cantabrian Mountain Range.

3. Materials and methods

3.1. Data acquisition

3.1.1. Passive cavity aerosol spectrometer probe (PCASP-X)

A *Passive Cavity Aerosol Spectrometer Probe*, *PMS Model PCASP-X* was installed close to the city of León, at 42° 36′ 30″ N, 5° 33′ 52″ W. This device measures particle sizes between 0.1 and 10 μm in 31 channels. Measurements were programmed continuously at intervals of 15 min every hour.

To compute the number of particles per unit of volume in each channel, a number of corrections had to be made, described in Calvo et al. (2013). Among these corrections, the refractive index (RI) is especially relevant because the PCASP-X is calibrated using latex particles, with a refractive index of 1.58-0i, so the size spectrum obtained initially refers to latex particles. Thus, in order to correct the raw size bins, two different refractive indices were estimated, corresponding to measurements carried out i) during biomass burning, and ii) before and after the wildfires:

i. For the measurements carried out during the two wildfires studied, a refractive index was estimated based on the results obtained by Levin et al. (2010) in lab tests for different types of fuel. This estimation takes into account the different types of trees burnt during the wildfire in Castrocontrigo: *Maritime pine*, *Scots pine*, *European black pine*, *Quercus pyrenaica*, *Quercus rotundifolia* and other riverside trees, considering the characteristic refractive index of each plant species, and the land area affected: 7835, 341, 719, 780, 416 and 5 ha, respectively. The refractive index obtained was $1.576 \pm 0.002–0.048 \pm 0.006i$. Table 1 shows the refractive index for the different types of fuel.
ii. For the measurements carried out before and after the arrival of the smoke plumes to the city, the refractive index was estimated from aerosol composition of PM_{10} based on the methodology developed by Levin et al. (2010). This methodology assumes that PM_{10} constituents are present as particular chemical compounds with a typical refractive index. Thus, the dry aerosol complex refractive index is calculated using Eqs. 1 and 2 from Hasan and Dzubay (1983). The PM_{10} filters for gravimetric mass analysis were collected during the measurement campaign of atmospheric aerosol conducted in

Table 1
Values of the refractive index and density for different fuel types (Levin et al., 2010) and estimated values for this study.

Fuel types	Percentage of mass	Refractive index		Density (kg m^{-3})
		Real part	Imaginary part	
Maritime pine	0.7760	1.577	0.05*i*	1265
Scots pine	0.0338	1.577	0.05*i*	1265
European black pine	0.0712	1.577	0.05*i*	1265
Pyrenean oak	0.0773	1.570	0.03*i*	1360
Quercus rotundifolia	0.0412	1.570	0.03*i*	1360
Other species	0.0005	1.570	0.03*i*	1360
Estimated values for this study (mean ± std)		1.576 ± 0.002	0.048*i* ± 0.006*i*	1276.00 ± 0.03

July 2012 in the city of León (Alves et al., 2014). The refractive index obtained was 1.549–0.025*i* (Castro et al., 2015).

From the two refractive indices estimated, the raw size bins were corrected by means of an algorithm based on Mie Theory (Bohren and Huffman, 1983).

3.1.2. Meteorological data

AEMET provided all the data on temperature, relative humidity, precipitation, atmospheric pressure, wind speed and direction, and visibility, through the weather station located at the airport of León. The meteorological data were provided in 10-min intervals, except for wind direction (every hour) and visibility (data corresponding to 0600, 0700, 0900, 1200, 1300, 1500 and 1800 UTC).

3.1.3. Wildfires: data

The Department for the Environment of the Regional Government Junta de Castilla y León provided all the information on the two wildfires analyzed in this paper (one registered in Cubo de Benavente and the other one in Castrocontrigo): area and district where the fires were registered, date of detection and extinction, total duration of the wildfire, and land area affected (ha) according to the type of vegetation burnt during the study period.

The wildfire in Cubo de Benavente was detected on 18 August 2012 at 1519 UTC and it was extinguished on 21 August at 1100 UTC. This town lies in the province of Zamora, to the south-west (SW), at about 70 km in a straight line from the city of León. This fire burnt 824 ha, of which 650 ha corresponded to forests (195 ha of trees and 456 ha of bushes and pasture) and 173 ha to other types of vegetation.

The wildfire in Castrocontrigo was detected on the 19 August 2012 at 1206 UTC and was extinguished on the 6 September at 1630 UTC. This town lies in the province of León, also to the SW of the city of León, at about 70 km from the city in a straight line. These two bordering towns, Cubo de Benavente and Castrocontrigo, lie in different provinces, but they are only 7 km apart. The fire in Castrocontrigo burnt a total of 11,768 ha, of which 11,592 ha corresponded to forests (10,096 ha were trees and 1496 ha bushes and pasture) and 176 ha were other types of vegetation. This was the largest wildfire ever recorded in the region of Castilla y León.

3.1.4. Air Quality Control Network in the City of León

The Air Quality Control Network of the City of León owns three monitoring stations, following the European Norm 1999/30/CE, in accordance with the number of inhabitants: a traffic station (LEO1), an urban background station (LEO3) and a suburban station (LEO4). Detailed information on the atmospheric pollutants measured by these stations and their spatial distribution in the city of León can be found in the URL of the district of León: http://www.aytoleon.es/.

The data on air quality used for this paper were obtained from the urban background station LEO3 for the pollutants NO, NO_2, SO_2, PM_{10}, and O_3. This station lies 50 m from the PCASP-X site. The data for the pollutants CO and $PM_{2.5}$ (which are not measured by the station LEO3) were provided by the traffic station LEO1 and by the suburban station LEO4, respectively. All the data were provided every hour.

3.2. Methodology

3.2.1. Optical parameters

The coefficients of scattering, absorption, extinction and backscattering (b_{scat}, b_{abs}, b_{ext} and b_{bscat}, respectively) and their mass efficiencies *MSE*, *MAE*, *MEE* and *MBSE*, respectively, have been estimated following the method described in Seinfeld and Pandis (2012) and also used by other authors, such as Hansell Jr et al. (2011), Levin et al. (2010) and Jung et al. (2009). The coefficients were computed from the efficiency of the scattering (Q_{scat}), absorption (Q_{abs}), extinction (Q_{ext}), and backscattering (Q_{bscat}), according to Mie theory, for the visible light spectrum (440, 670 and 870 nm), respectively.

To compute the mass efficiencies, the particulate matter has been estimated from the aerosol size distributions considering the density corresponding to each type of measured aerosol:

i. In the measurements influenced by the wildfires of Cubo de Benavente and Castrocontrigo the aerosol density used was 1276 kg m^{-3} (Table 1). This density was estimated following the same method as for the refractive index (Levin et al., 2010), described in Section 3.1.1. Our estimation is in agreement with the study on aerosol from biomass burning by Reid et al. (2005).
ii. In the measurements that were not influenced by the two wildfires, the density of the urban aerosol used was 1940 kg m^{-3} (Castro et al., 2015). This density was derived from aerosol composition, following Levin et al. (2010), as mentioned in Section 3.1.1. The composition was obtained from the chemical analysis of filters collected during the measurement campaign of atmospheric PM carried out in July 2012 in the city of León (Alves et al., 2014; Castro et al., 2015). This result is similar to other measurements of urban aerosol density (Pitz et al., 2003).

RI for biomass burnings smokes used in this study has been calculated in reference to Levin et al. (2010), where refractive indices for different types of fuels are the results of combustion chamber experiments under a controlled atmosphere. The calculated refractive index of 1.576–0.048*i* is in the range of the real (1.55 to 1.80) and imaginary (0.01 to 0.50) parts found by Levin et al. (2010) for visible wavelength. Hungershoefer et al. (2008) also reported a possible range of 1.41 to 1.60 for real part and 0.0093 to 0.1 for the imaginary part of the refractive index for biomass burning emissions. Schkolnik et al. (2007) reported refractive indices for main chemical components EC and OC in biomass burning aerosols ($\rho_{EC} = 1.8$ g cm^{-3} and $RI_{EC} = 1.87–0.22i$, and $\rho_{OC} = 0.9$ g cm^{-3} and $RI_{OC} = 1.4 - 0i$). Moreover, Adler et al. (2010) determined an effective refractive index for OC in fresh diesel soot of $1.519 + 0.048i$, conferring an absorbing property to the organic carbon. Our dry refractive index is thus representative of fresh biomass burning smoke without considering the possible evolution of the optical properties, first in the fire area through the combustion efficiency, and secondly, during transport from the fire area to the sampling area, through water uptake and chemical aging.

3.2.2. Radiative forcing: global atmospheric model (GAME)

Aerosol-related optical parameters such as Atmospheric Optical Depth (AOD), Single Scattering Albedo (SSA) and asymmetry parameter (g) are necessary to perform radiative transfer calculations. As the last

two parameters were not directly measured, we have estimated them using Mie theory with aerosol size distribution and with the refractive index, every 3 h between 0700 UTC and 1600 UTC for each sampling day. Thus, SSA and *g* have been estimated at the seven wavelengths used in the GAME radiative transfer model. Concerning the AOD parameter, every time AERONET data were available, we referred to and computed spectral dependence following the extinction efficiency spectral dependence given by Mie calculations. The closest AERONET site considered here is located in Palencia (around 150 km eastward from the wildfires and highly influenced by smokes during wildfires episodes). Necessary surface albedos are also extracted from these level 1.5 AERONET data. Atmospheric aerosol stratification is established thanks to the closest radiosounding existing as described in Section 3.2.3, and following these rules: i) in the Atmospheric Boundary Layer (ABL), the AERONET AOD is vertically distributed, and spectral dependence for AOD, *g* and SSA is given by Mie calculations; ii) upper layers data (between top of ABL and Top Of the Atmosphere (TOA)) are derived from AOD, SSA and *g* data given by Hess et al. (1998); continental average (between top of ABL and around 2 km), free troposphere (2–12 km) and stratosphere (12-TOA) aerosol types are considered.

The instantaneous clear-sky direct radiative forcing has been estimated from the GAME radiative transfer model, detailed in Dubuisson et al. (2004). Scattering and absorption by aerosols, clouds and molecules are taken into account. Upward and downward net radiative fluxes are calculated over the spectral solar range, from 2500 to 50,000 cm^{-1}, with a 100 cm^{-1} spectral resolution. Calculations of radiative fluxes integrated over the entire shortwave region are performed at the specific sampling time. We have computed the aerosol clear-sky daytime direct radiative forcing at the bottom of atmosphere (Kim and Boatman, 1990), ΔFBOA, at TOA (20 km in this case), ΔFTOA and the atmospheric forcing, ΔFATM, which represents the possible absorption of solar radiations due to absorbing properties of fire particles within the atmospheric layer where aerosols are located. More information on GAME Model and past uses can be found in Stamnes et al. (1988), Dubuisson et al. (1996), Calvo et al. (2010) or Alonso-Blanco et al. (2014).

3.2.3. Thermal inversions and circulation weather type classification and air mass

In order to identify the type of weather associated to a particular synoptic situation a Circulation Weather Type classification (CWTs) was carried out based on Jenkinson and Collison (1977) and Jones et al. (1993). These procedures were developed to define objectively Lamb Weather Types for the British Isles (Lamb and Britain, 1972). Nevertheless the procedure can be easily applied to other areas (Goodess and Jones, 2002). The daily circulation affecting the Iberian Peninsula is described using a set of indices associated to the direction and vorticity of the geostrophic flow (Fernández-González et al., 2012).

Tracks of the smoke plumes from the two wildfires have been identified by means of HYSPLIT (Hybrid Single Particle Lagrangian Integrated Trajectory Model) by the NOAA (Draxler and Rolph, 2013; Rolph, 2013).

The HYSPLIT Trajectory Model enabled us to identify the origin of the air masses by means of back-trajectories of 72 h (3 days) computed at 750, 1500 and 2500 m AGL. The air masses were classified into sectors according to their origin: Atlantic North (AN), Atlantic Northwest (Mauzerall et al., 1998), Atlantic West (AW), Atlantic Southwest (Forster et al., 2007), North Africa (AFR), Mediterranean (MED), Europe (E.E.A. (E.E.A. (European Environment Agency), 1999) and Regional (REG). This classification has already been employed in other studies, including Coz et al. (2009), Dimitriou et al. (2016), Papadopoulos et al. (2014) and Salvador (2004).

In addition, the HYSPLIT Dispersion Model was used to compute the dispersion of the emissions released by the wildfires. This model was implemented by the global aerosol model Navy Aerosol Analysis and Prediction System (NAAPS) from the Naval Research Laboratory (NRL) in Monterrey, California (EEUU) (Christensen, 1997). This later provided the smoke concentration at surface level.

The thermal inversions were computed using data from the closest radiosounding, the one in Santander (43.48° N, 3.80° W, altitude 59 m ASL), provided by the University of Wyoming (http://weather.uwyo.edu/upperair/sounding.html).

3.2.4. Inhalable, thoracic, tracheobronchial and respirable fractions

The aerosol size fractions associated with health problems were evaluated in accordance with the Spanish standard UNE 77213, which is equivalent to ISO 7708 (1995). These standards define conventions for atmospheric particle size fractions for use in assessing possible health effects in the workplace and ambient environment. The conventions specify the relationships between aerodynamic diameter and aerosol fractions collected or measured by the sampling instrument. These fractions represent approximately the part that reaches, under average conditions established by ISO 7708 (1995), different regions of the respiratory tract. Particle sampling conventions have been established, expressed as curves describing penetration to the region of interest in terms of the particle aerodynamic diameter. From the experimental size distributions, first, the inhalable and thoracic fractions, and then the tracheobronchial and respirable fractions were assessed for healthy adults and high-risk groups (children, elderly or infirm people). This methodology has been used in previous studies (Castro et al., 2015).

4. Results and discussions

4.1. Transport and dispersion of the smoke plumes

The analyses of the circulation weather types, air masses and thermal inversions have revealed how the smoke plumes from the wildfires arrived to the city of León.

The weather type on 18 August 2012 was “hybrid Anticyclonic Southwestern”. However, on 19 and 20 August the weather type was “no directional Anticyclonic (A)”, turning into “pure Northeastern (NE)” on 21 and 22 August 2012 (Table 2).

After the formation of the pyrocumulus, the smoke plume went directly to León (Fig. S1). Backward trajectories (Fig. 1) and satellite images (Fig. S2) confirm this fact. Backward trajectories show how the smoke plumes from the wildfires are carried directly towards the city (Fig. 1). The change of air masses towards the Atlantic Western sector (AW) was the reason why the smoke plume did not reach the city on the 22 August, and the levels of pollutants decreased and the subsidence inversion disappeared in the lower layers of the atmosphere.

Besides, the HYSPLIT *dispersion* model indicates that the smoke plumes moved towards the north-east (NE), from the surface level to an altitude of 750 m AGL, on the 19, 20 and 21 August 2012, reaching the whole of the city of León. The NAAPS model also shows the presence of smoke at surface level on those days. Fig. 2 shows an example of both models for the 20 August.

The radiosoundings launched in the city of Santander showed the presence of intense subsidence inversions typical of an Anticyclonic situation from 1200 UTC on 19 August, at altitudes close to surface level (235 m and 366 m) (see Fig. S3). In addition, on the 20 and 21 August we find radiative inversions below 200 m at 0000 UTC. The joint action of these inversions (Table 2) hinder the vertical dispersion of the smoke plumes from the two wildfires from the last hours of the 19 and, more particularly, on the 20 and 21 of August. The smoke plume spread only horizontally, as shown in Fig. 2, leading to the severe air-pollution event studied in the city. The information available states that the 18 of August is the day prior to the event. The actual event began in the evening of the 19 and the situation continued developing until the 21 of August. On the 22 an Atlantic air mass entered the city of León, thus stopping the air-pollution event abruptly and the smoke plumes could not reach the city any longer.

Table 2
Circulation weather type (CWT) classification and radiative and subsidence thermal inversions on 18, 19, 20, 21 and 22 August 2012. The days in which León was affected by the forest fire plumes have been highlighted in bold.

Day	CWT	Thermal inversions			
		Santander 0000 UTC		Santander 1200 UTC	
		Radiative (m AGL)	Subsidence (m AGL)	Radiative (m AGL)	Subsidence (m AGL)
18/08/2012	ASW		612 and 1090		890
19/08/2012	**A**		**673, 1107 and 5627**		**235, 541 and 1686**
20/08/2012	**A**	**129**	**366, 1777 and 5554**		**1188**
21/08/2012	**NE**	**129**	**1349, 4002 and 5241**		**1408**
22/08/2012	NE	51	1659, 2172 and 4689		1815 and 4713

4.2. Meteorological study

According to the AEMET, the summer of 2012 was one of the driest summers in the past 60 years. In the month of August, when the two wildfires are registered, the precipitation was 3.05 mm in the AEMET station located at the airport of León, and the relative humidity was 15%. The normal values for that month are 24 mm and 56%, respectively, so there was an average decrease of 70%. All this implies atmospheric conditions favoring the occurrence of large wildfires.

Concerning the prevailing weather conditions of days 19, 20 and 21, the synoptic chart at sea level (Fig. S4) shows a poorly defined situation. One could speak of a flat low on the Iberian Peninsula. However, in the 850 and 700 hPa charts (Fig. S5) a more profiled layout is observed, with the isohypses showing a SW flow at heights of about 1600 and 3200 m. This wind direction coincides with the trajectories shown in Figs. 1, 2 and S2. In addition, the narrowness of the plume (Figs. 2 and S1) can be explained by the closeness of the isohypses (i.e., the gradient of the geopotential height) over the study area.

Fig. 3 shows the evolution of some meteorological variables on the study days. On the 20 and 21 of August there was a significant loss of visibility (Fig. S6) due to the high amounts of particulate matter (on average 1640 ± 570 particles cm^{-3} and 1720 ± 630 particles cm^{-3}, respectively) and gases released by the wildfires. On the 20 and 21 of August the visibility was 20 and 29 km, respectively, whereas on the day before it was of 63 km and on the day after it was of 78 km. In addition, on both days we find ash deposition processes on the ground and on cars in the city of León with cinders larger than 1 cm (Fig. S7 and S8). Considerable reduction in visibility due to long-range transported smokes emitted by biomass burning has also been described in Saarikoski et al. (2007).

The mean temperature during the 5 study days was around 23 °C, with maximum temperatures of 30 °C and minimum temperatures of 15 °C. There was no precipitation, and the average daily relative humidity between the 19 and 21 of August was between 32 ± 11 and 40 ± 14%. The low standard deviations indicate that there were virtually no changes in the relative humidity when the smoke plumes arrived to the city, in contrast with the results found by Saarikoski et al. (2007). On the 22 August, when the smoke plumes started to disperse, the average humidity increased to 46 ± 21% (with a maximum of 87%). This is the highest value registered during the study period and occurs as a result of the arrival of a different air mass from the Atlantic (AW sector).

The wind speed is similar on the 5 study days, with a daily average value of 3 m s^{-1} and a deviation of 1.3 m s^{-1}. This situation implies poor atmospheric ventilation, which makes the ambient situation over the city even worse. The estimated time the plumes took to reach the city was <7 h.

4.3. Implications of biomass burning in air quality

4.3.1. Particulate matter (PM)

The arrival of the smoke plumes to the city of León caused important changes in air quality indicators (Fig. 4). In the days with the highest levels of pollution, 20 and 21 of August, the daily average concentration of PM_{10} was 29 ± 20 and 32 ± 15 μg m^{-3}, respectively. These values imply an increase in PM_{10} of 30% and 122% when compared with the day before and the day after the event, respectively. The analysis of the evolution of aerosol concentrations during the study period revealed three hourly maximum values: two on the 20 August and one on the 21, with a high number of particles (Fig. 3), between 2150 and 3500 particles cm^{-3}. In these intervals, the PM_{10} concentrations were over 50 μg m^{-3}, but the daily threshold value (24 h) established by the Spanish law (*Real Decreto 102/2011, de 28 de enero*: 50 μg m^{-3}) was not exceeded during the study period. Authors such as Barnaba et al. (2011) and Amiridis et al. (2012) have found an evident impact of wildfires on PM_{10} values.

Something similar occurs with the concentration of $PM_{2.5}$. Before the smoke plume, the average concentration was below 4 μg m^{-3}, whereas on the days with the highest levels of pollution, 20 and 21 August, the daily concentration reached average values between 9 and 13 μg m^{-3}, with an hourly maximum of 36 μg m^{-3}. Important increases of $PM_{2.5}$ associated to biomass burning have also been found by Saarikoski et al. (2007) and Alves et al. (2010).

4.3.2. Gases

The wildfires studied in this paper also triggered significant changes in the atmospheric gases. On the 20, 21 and 22 of August, between 0700 and 1000 UTC, we found NO concentration peaks between 11 and 19 μg m^{-3} from the emissions of road traffic. However, the 18 and 19 were non-working days, so the emissions of NO were very low and no such peaks were registered. The most important increase in NO registered in the whole study period occurred on 20 of August between 1800 and 2100 UTC. The average NO concentration was 15 ± 11 μg m^{-3}, with a maximum of 29 μg m^{-3} at 2000 UTC. These values do not follow the normal daily pattern determined by road traffic, but must rather be attributed to the wildfires as it coincides with the peak in PM_{10} registered at the same time.

With respect to the concentration of NO_2, two peaks were registered which may be due to road traffic emissions. The first peak was registered at dawn (between 0400 and 0900 UTC) and occurred at the same time as the NO emissions. The second peak was registered in the evening (between 1900 and 2300 UTC), possibly as a result of direct oxidation of NO into NO_2. As a consequence, this second peak was not found for the NO concentrations. The average concentrations found in these two peaks lie between 8 ± 2 μg m^{-3} on 19 of August and 39 ± 25 μg m^{-3} on the day after. On 20 of August, at the time of the maximum concentration of NO, between 1800 and 2100 UTC, the maximum NO_2 concentration in the whole study period was registered, exceeding 60 μg m^{-3}, with an average value of 54 ± 11 μg m^{-3}.

The emissions of NO_x during the wildfires are associated with complete combustion during the flaming phase (Amaral et al., 2014). This situation is described by Delmas et al. (1995) who found a good correlation between CO_2 and NO_x during biomass burning in the Tropical African Savanna. The results obtained in relation with the content of NO_x demonstrated the existence of the flaming phase, but the data available

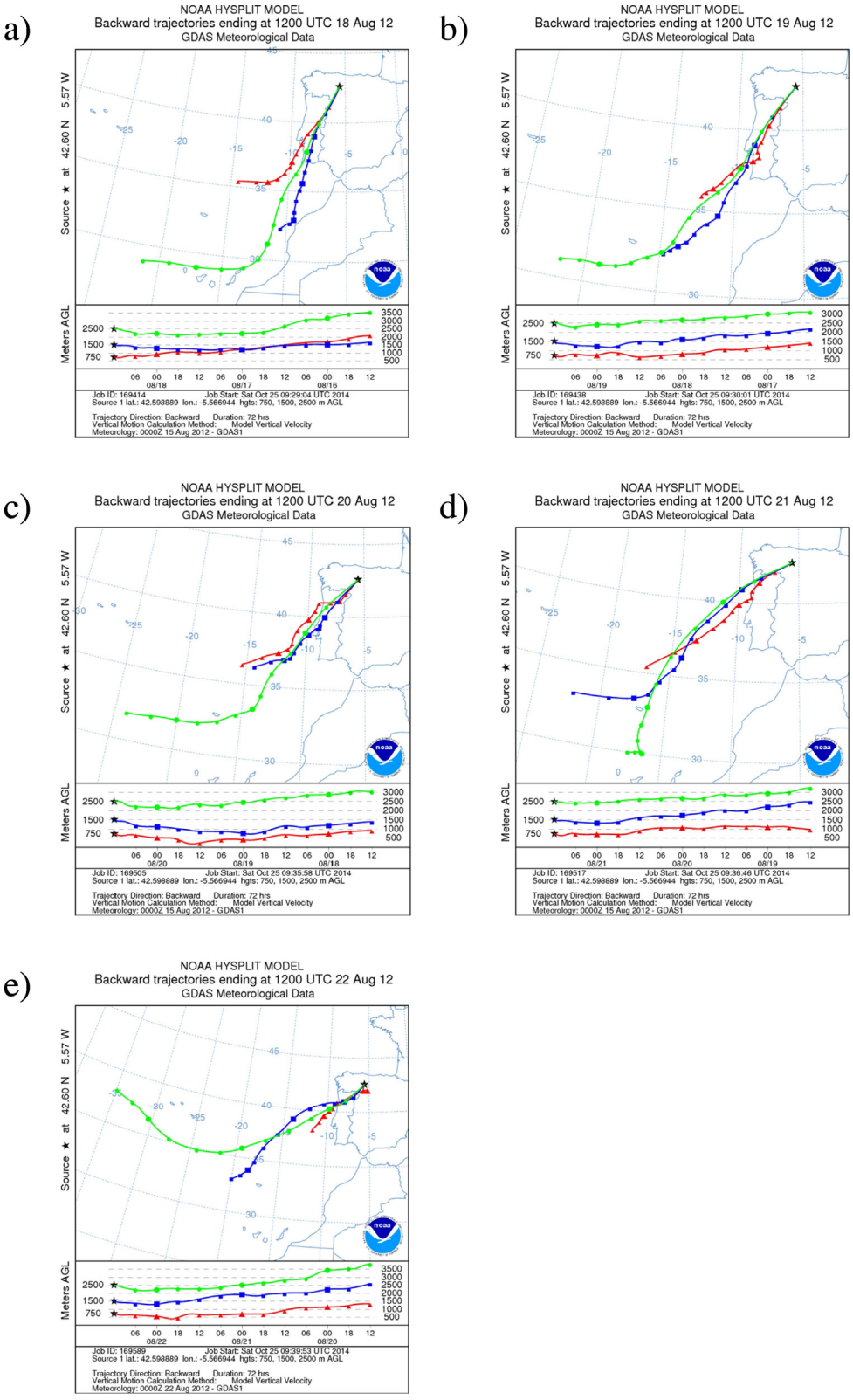

Fig. 1. Backward trajectories for three different altitudes (750, 1500 and 3000 m) using the HYSPLIT model on (a) 18, (b) 19, (c) 20, (d) 21 and (e) 22 August 2012 carried out at 1200 UTC for 72 h.

do not enable us to identify the periods in which this particular phase was dominant.

Changes in the concentrations of tropospheric ozone (Liu et al., 1999) were also found, though indirectly and in association with the chemical reactions in the atmosphere involving the gases released during the wildfires. On the days on which the wildfires did not affect the urban particulate matter, the highest O_3 concentration was registered during the day, between 0700 and 1900 UTC, with an average value of around 90 μg m^{-3}. The maximum O_3 concentration was reached between 1300 UTC and 1400 UTC, with values between 115

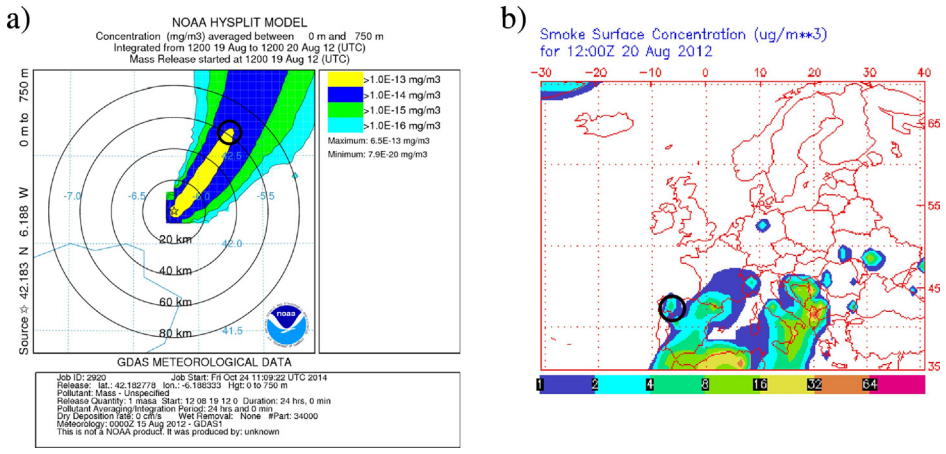

Fig. 2. Example of a) dispersion of the smoke plume from the wildfire in Castrocontrigo obtained by the HYSPLIT dispersion model, and b) NAAPS model results showing surface smoke concentrations (in μg m^{-3}) on 20 August 2012. The center of the black circle is the city of León.

and 126 μg m^{-3}. This pattern is not found on the days when the smoke plumes reach the city, as the O_3 concentration during the day (between 0700 and 1900 UTC) was under 90 μg m^{-3} (Fig. 4). As mentioned in Section 4.2, there was a noticeably reduced visibility on those days because of the particulate matter and gases released by the wildfires. The decrease in solar radiation due to the emissions from the wildfires in these days may be inhibiting the formation of tropospheric ozone by means of photocatalytic processes in the lower layer of the troposphere. Authors such as Deng et al. (2008) have found an average daily decrease in the concentration of tropospheric ozone from 36 to 11 ppbv when comparing conditions with no fire and conditions with a fire close by, respectively. This might be a consequence of the reduced solar radiation caused by the emissions from wildfires. Besides, the drop in the concentration of O_3 points towards direct oxidation of NO into NO_2. Similar situations have also been described by other authors. Amiridis et al. (2012) found in Athens that the arrival of a smoke plume from biomass burning triggered an increase in NO_x in the weather station closest to the plume, rising from 10 to 94 μg m^{-3}, while the O_3 concentration dropped by 50 μg m^{-3}. Rissler et al. (2004) have also found a decrease in O_3 as a result of NO oxidation in recent biomass burning events in the Amazon rain forest.

As far as the concentrations of CO and SO_2 are concerned, there was a significant increase in the concentration of CO on the 20 August between 1800 and 2100 UTC, the highest amount registered in the study period, with over 0.60 mg m^{-3}. The values of SO_2 concentrations provided by the air-quality network did not suggest a clear influence of the wildfires in the case of this particular gas (Fig. 4).

The maximum values found in the concentrations of NO_x coincided with the maximum concentration of PM_{10} and CO in the study period, and with the minimum concentration of O_3. This coincidence in four major pollutants suggests the influence of the wildfires.

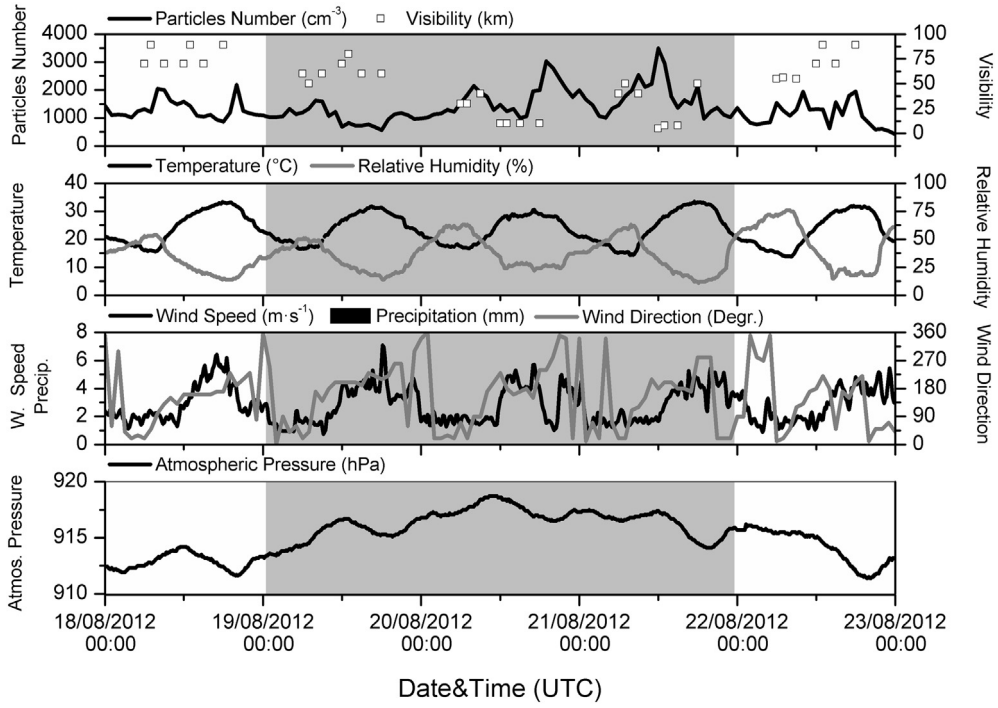

Fig. 3. Meteorological study with data on visibility, temperature, relative humidity, wind speed and wind direction, precipitation and atmospheric pressure as well as the evolution of the number of particles during the five study days. The shaded area corresponds to the days when the smoke plumes arrived in the city of León.

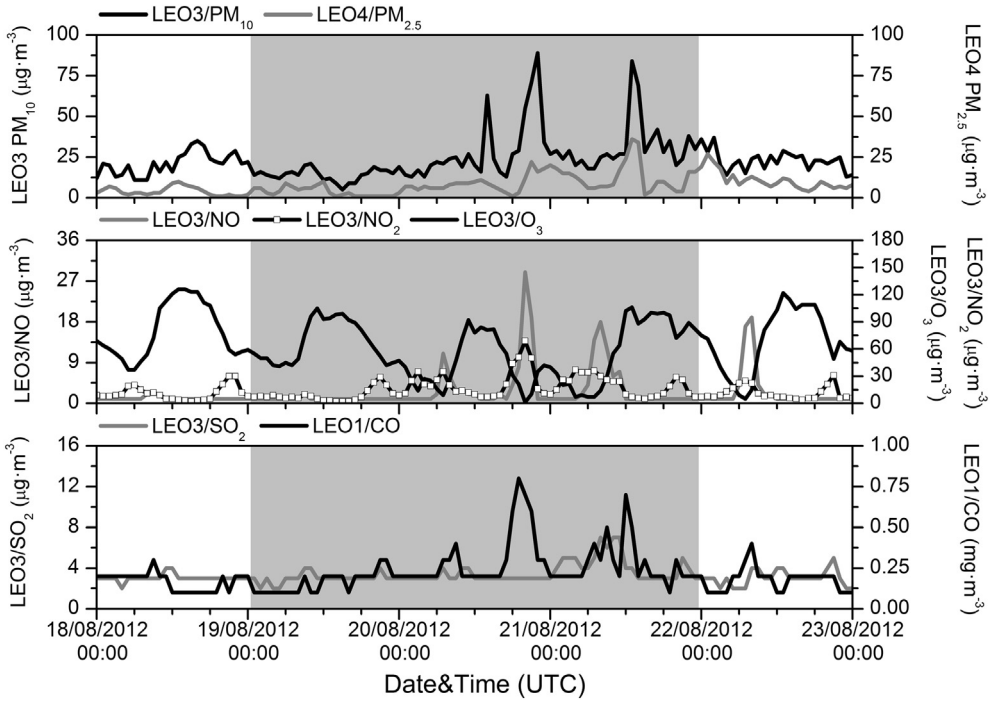

Fig. 4. Air quality data provided by the air Quality Control Network of the City of León for the 5 study days: concentration of NO, NO_2, SO_2, PM_{10}, and O_3 measured at station 3 (LEO3), concentration of CO measured at station 1 (LEO1) and $PM_{2.5}$ measured at station 4 (LEO4). The shaded area corresponds to the days when the smoke plumes arrived in the city of León.

4.4. Influence of biomass burning on number, surface and volume distributions

The changes in the physical properties of the aerosols in the three days in which the smoke plumes affected the city have been studied through aerosol size, surface and volume distributions (Fig. 5). The number of particles (N_t), surface area (S_t) and volume (V_t) have been analyzed, as well as their corresponding count, surface and volume median diameters (CMD_t, SMD_t and VMD_t) and their geometric standard deviations (σ_{gt}) for the total aerosol size distribution and for the fine (N_f, S_f and V_f) and coarse (N_c, S_c and V_c) modes (Table 3).

On the 19, 20 and 21 August there was an important increase in N_t with a daily average of 1050 ± 280, 1640 ± 570 and 1720 ± 630 particles cm^{-3}, respectively, with maximum concentrations between 2150 and 3500 particles cm^{-3}. Considerable increases in particles due to biomass burning have also been found by Rissler et al. (2006). These authors have found a direct relationship between the increase in the number of particles in the submicrometric fraction (30–850 nm) and the occurrence of wildfires.

As for the whole aerosol size distribution, the number of particles in the fine mode changed dramatically (Fig. 5a) in the days with higher levels of pollution: 20 and 21 August. However, on 20 August this increase is particularly significant for particles smaller than 0.2 μm, whereas on 21 August the increase is more significant in particles larger than 0.2 μm.

With respect to the fine mode, the study reveals that in these three days the CMD_f increased gradually (0.09, 0.11 and 0.14 μm, respectively), pointing towards an increase in particle size as the smoke plumes arrived in the city (Table 3). These results are consistent with the estimation of the mass fraction from the data provided by the PCASP with average PM_1 values of 2.5 ± 0.7, 4.5 ± 1.7 and 6.6 ± 4.1 μg m^{-3}, respectively (considering a density of 1276 kg m^{-3}). Other studies, such as Deng et al. (2008), Janhäll et al. (2010) and Okoshi et al. (2014), have also noted that biomass burning triggered an increase in the number of particles in the fine mode.

Three maximum particle concentrations were identified in the three study days: two on 20 August at 0800 and 1900 UTC, and one on 21 August at 1200 UTC, with particle concentrations of 2145, 3029, and 3492 cm^{-3}, respectively. The CMD_f in these measurements was 0.11, 0.12 and 0.19 μm, respectively. These size distributions have the same pattern: an increase in the number of particles smaller than 1 μm, which is even more important in the largest fraction of the fine mode as the CMD_f increases. This is consistent with the daily average values on 20 and 21 August.

The day after the pollution event (22 August) the daily average CMD_f changed with respect to the previous day. The CMD_f is reduced to 0.13 ± 0.02 μm probably as a consequence of the change in the air masses observed this day, suggesting a halt in the arrival in the city of smoke plumes from those particular wildfires.

The number of particles larger than one micron (coarse mode) may seem irrelevant, but these particles contribute greatly to the total mass, accounting for up to 96% of the total during the main pollution peaks due to particulate matter.

The behavior of the chemical particulate content during this pollution event may be attributed to several factors: i) different types of fuel, ii) predominance of the flaming phase over smoldering, or vice versa, and iii) aerosol aging processes. The reduced vertical dispersion in the study days, as shown by the weather data, causes a longer permanence of aerosols in the atmosphere, and this in turn implies a higher degree of oxidation.

The aerosol surface and volume distributions (Fig. 5b and c) also changed during the fire event. These changes can be mainly attributed to the fine mode. As the smoke plumes from the wildfires arrived in the city of León, the area and volume distributions increased for particles <0.3 μm. This increase was more remarkable during the days with the highest concentrations of particles in the largest fraction of the fine mode: between 0.2 and 0.3 μm. The following day we found a decrease in the area distribution and volume for sizes both smaller than 0.3 μm and larger than 0.3 μm. This may be due to the change in the nature of particles after the arrival of Atlantic air masses.

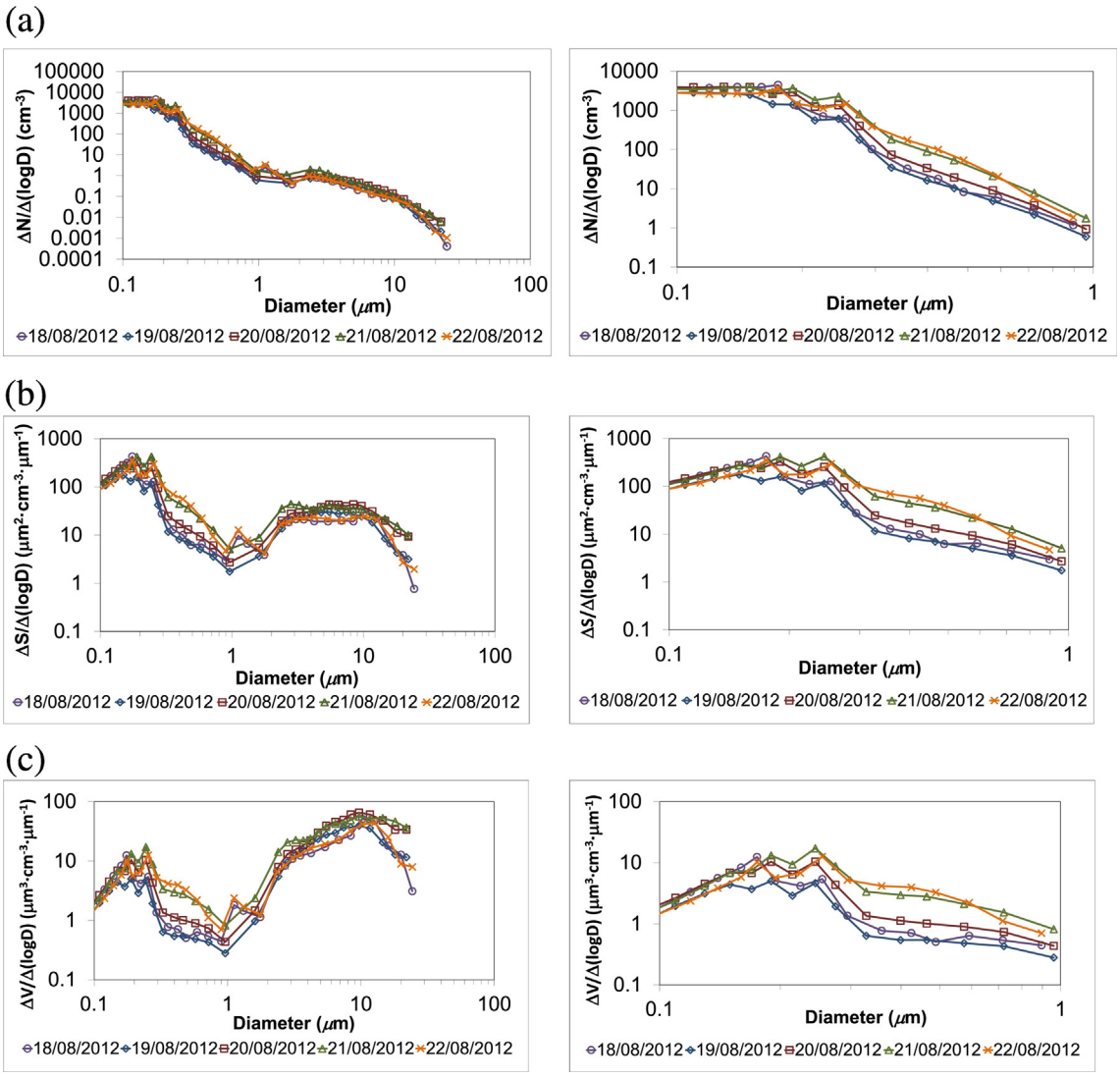

Fig. 5. Aerosol (a) size, (b) surface and (c) volume distributions for the total aerosol distribution, and the one corresponding to the fine mode (particles size <1 μm) registered on 18, 19, 20, 21 and 22 August 2012.

In the city of León, during the days affected by the wildfires (19 to 21 August), there was a gradual increase in aerosol volume and surface area, from 87 ± 26 to 179 ± 89 $\mu m^2\ cm^{-3}$, and from 25 ± 13 to 45 ± 23 $\mu m^3\ cm^{-3}$, respectively.

For further study of aerosol size distributions, it is necessary to take into account two aspects: i) the processes involved (condensation, coagulation and aging processes among others) together with the gases emitted during the combustion and ii) the technique used to classify aerosols (particle optical, aerodynamic, equivalent mobility or geometric size) (Reid et al., 2005). Nevertheless, in any case, all authors agree that freshly released aerosols are smaller than aged aerosols (Wardoyo et al., 2007; Capes et al., 2008; Janhäll et al., 2010; Hsiao et al., 2016).

4.5. Optical properties of aerosols from biomass burning and associated radiative forcing

The aerosol optical properties and the associated radiative forcing have been estimated for the visible light spectrum.

4.5.1. Optical properties of aerosols from biomass burning

It was found that the shorter the input wavelength, the higher the b_{scat}, b_{abs}, b_{ext} and b_{bscat} (Table 4) estimated. For example, for the total particle distribution and a wavelength of 870 nm, in the four coefficients analyzed in the study period, an average decrease of 37 ± 15% was found in relation with the wavelength of 440 nm. In the fine mode the decrease was more pronounced than in the coarse mode. This is due to the strong dependence of the four coefficients between the wavelength and the particle size (Seinfeld and Pandis, 2012), which has been observed in other studies, such as Reid and Hobbs (1998) or O'Neill et al. (2002).

MSE, MAE, MEE and MBSE are conditioned by the values of b_{scat}, b_{abs}, b_{ext} and b_{bscat}, and for the total particle distribution and a wavelength of 870 nm there was a decrease of 32 ± 22% when compared with a wavelength of 440 nm. However, the strong dependence on the mass distribution (Seinfeld and Pandis, 2012) makes the estimated values of these parameters for the same wavelength higher in the fine mode than in the coarse mode (Table 5).

The influence of the smoke plumes arriving in León on the optical properties of urban aerosol has been analyzed for a wavelength of 670 nm (central wavelength of the three considered in this paper).

Both b_{scat} and b_{abs} increased gradually during the pollution event, with a daily average of 28 ± 22 Mm^{-1} and 16 ± 10 Mm^{-1}, respectively. And so did b_{ext} (b_{scat} + b_{abs}). This situation was due to a considerable

Table 3
Number of particles (N_t), surface area (S_t) and volume (V_t) and their corresponding Median Diameter (CMD_t, SMD_t and VMD_t) and Geometric Standard Deviation (σ_g) for the total aerosol size distribution on each day, and for the fine mode (N_f, S_f, V_f) and the coarse mode (N_c, S_c, V_c). In bold the days in which León city was affected by the forest fire plumes.

Day	Total aerosol size distribution								
	N_t (cm^{-3})	CMD_t (μm)	σ_{gt}	S_t ($\mu m^2\ cm^{-3}$)	SMD_t (μm)	σ_{gt}	V_t ($\mu m^3\ cm^{-3}$)	VMD_t (μm)	σ_{gt}
18/08/2012	1321 ± 347	0.14 ± 0.01	1.31 ± 0.01	113 ± 24	0.32 ± 0.10	4.03 ± 1.09	26 ± 12	5.18 ± 1.72	4.09 ± 1.09
19/08/2012	**1045 ± 277**	**0.13 ± 0.00**	**1.36 ± 0.02**	**87 ± 26**	**0.38 ± 0.08**	**4.79 ± 0.68**	**25 ± 13**	**5.56 ± 1.42**	**3.25 ± 0.43**
20/08/2012	**1641 ± 566**	**0.13 ± 0.01**	**1.38 ± 0.02**	**146 ± 60**	**0.36 ± 0.07**	**4.50 ± 0.73**	**43 ± 31**	**5.85 ± 1.78**	**3.44 ± 0.43**
21/08/2012	**1717 ± 632**	**0.14 ± 0.01**	**1.42 ± 0.05**	**179 ± 89**	**0.37 ± 0.05**	**4.19 ± 0.64**	**45 ± 23**	**5.60 ± 1.39**	**3.65 ± 0.44**
22/08/2012	1142 ± 415	0.16 ± 0.01	1.42 ± 0.04	129 ± 36	0.36 ± 0.06	3.65 ± 0.88	28 ± 13	4.65 ± 1.99	4.12 ± 0.81
Day	Fine mode								
	N_f (cm^{-3})	CMD_f (μm)	σ_{gf}	S_f ($\mu m^2\ cm^{-3}$)	SMD_f (μm)	σ_{gf}	V_f ($\mu m^3\ cm^{-3}$)	VMD_f (μm)	σ_{gf}
18/08/2012	1320 ± 347	0.14 ± 0.01	1.33 ± 0.04	93 ± 24	0.18 ± 0.01	1.61 ± 0.08	3 ± 1	0.22 ± 0.01	1.66 ± 0.10
19/08/2012	**1044 ± 277**	**0.09 ± 0.01**	**1.75 ± 0.04**	**66 ± 18**	**0.16 ± 0.01**	**1.78 ± 0.05**	**2 ± 1**	**0.22 ± 0.01**	**1.85 ± 0.06**
20/08/2012	**1640 ± 566**	**0.11 ± 0.02**	**1.67 ± 0.06**	**114 ± 41**	**0.18 ± 0.01**	**1.71 ± 0.04**	**4 ± 1**	**0.23 ± 0.01**	**1.76 ± 0.05**
21/08/2012	**1716 ± 632**	**0.14 ± 0.02**	**1.63 ± 0.05**	**145 ± 73**	**0.20 ± 0.01**	**1.68 ± 0.05**	**5 ± 3**	**0.26 ± 0.02**	**1.72 ± 0.07**
22/08/2012	1141 ± 416	0.13 ± 0.02	1.78 ± 0.09	108 ± 30	0.24 ± 0.03	1.93 ± 0.15	4 ± 1	0.26 ± 0.02	1.67 ± 0.09
Day	Coarse mode								
	N_c (cm^{-3})	CMD_c (μm)	σ_{gc}	S_c ($\mu m^2\ cm^{-3}$)	SMD_c (μm)	σ_{gc}	V_c ($\mu m^3\ cm^{-3}$)	VMDc (μm)	σ_{gc}
18/08/2012	1 ± 0	1.71 ± 0.08	1.84 ± 0.08	20 ± 10	5.51 ± 2.03	2.52 ± 0.45	23 ± 12	7.45 ± 1.10	2.17 ± 0.12
19/08/2012	**0 ± 0**	**2.82 ± 0.12**	**1.67 ± 0.05**	**21 ± 9**	**5.58 ± 0.86**	**1.88 ± 0.12**	**23 ± 12**	**7.46 ± 1.31**	**1.83 ± 0.08**
20/08/2012	**1 ± 0**	**2.78 ± 0.19**	**1.63 ± 0.11**	**32 ± 20**	**5.54 ± 0.84**	**1.92 ± 0.13**	**39 ± 30**	**7.08 ± 1.42**	**1.84 ± 0.10**
21/08/2012	**1 ± 1**	**2.59 ± 0.15**	**1.62 ± 0.08**	**35 ± 18**	**5.20 ± 1.02**	**1.94 ± 0.16**	**40 ± 21**	**7.27 ± 1.25**	**1.91 ± 0.11**
22/08/2012	1 ± 0	2.82 ± 0.22	1.56 ± 0.08	21 ± 11	5.93 ± 1.69	1.83 ± 0.21	24 ± 13	6.43 ± 1.54	2.22 ± 0.22

increase in the particle concentration as the smoke plumes arrived in the city. Simultaneously, the number and size of the particles also increased, as described above. Table 4 shows that the standard deviation of b_{scat} and b_{abs} also increased gradually as the smoke plumes arrived. This might be attributed not only to the changes of characteristics in number distribution of aerosols during the pollution event, but also to the increase of the real and imaginary part of the calculated refractive index for this smoke episode.

b_{scat} is the main contributor to b_{ext}. This contribution is about 10% lower on the days when the smoke plumes arrive in the city when compared with other days. Aerosols became more absorbing in relation to the incoming of smoke plumes containing carbonaceous aerosols as imaginary parts of the calculated refractive index showed. b_{bscat} had very low values during the study period, never exceeding 0.7 ± 0.4 Mm^{-1}. The same situation was found in the fine mode.

With smoke plumes in the city, the values of MSE and MAE of the total distribution of aerosol were higher than the day before and the day after the arrival of the smoke plumes. The days when the smoke plumes arrived, MSE ranged between 0.34 and 0.38 $m^2\ g^{-1}$ and MAE between 0.23 and 0.26 $m^2\ g^{-1}$, whereas the previous and following days these parameters were 0.24 and 0.34, and 0.12 and 0.13 $m^2\ g^{-1}$, respectively (Table 5). During the days influenced by the smoke plumes there was no rising trend in MSE and MAE, contrary to what happened with b_{scat} and $b_{abs,}$ mainly because of the strong dependence of the former on the aerosol mass distribution. MBSE also followed the same trend found for MEE and MAE, with very low values never exceeding 0.1 $m^2\ g^{-1}$.

In the fine mode, the values of MSE and MAE estimated were higher than in the coarse mode because most of the mass fraction belongs to the latter. In both modes, MSE and MAE, and total particle distribution, were up to 33% higher when the smoke plumes arrived in the city. The average values of MSE and MAE in the fine mode were 1.7 ± 0.17 and 0.76 ± 0.02 $m^2\ g^{-1}$, respectively, and 0.21 ± 0.03 and 0.18 ± 0.02 $m^2\ g^{-1}$, respectively, in the coarse mode. The values estimated in this paper are consistent with the values found in the relevant literature (Reid et al., 2004; Reid et al., 1998). A high particle number concentration in the largest fraction of the fine mode may lead to higher values in the MSE, as shown by Reid et al. (2004). Reid et al. (1998) found an increase in MSE in aged smoke plumes when compared with fresh smoke in different wildfires in Brazil. Moreover, Cheng et al. (2014) found that MSE values increased rapidly with increasing mass concentration in low aerosol loading as in this case study.

The many variables that determine the optical properties of the aerosols released by the wildfires, such as particle size, composition, density or particle refractive index, imply many uncertainties in the analysis. This causes discrepancies between the many authors who have approached this research topic. The discrepancies are related not only to the characteristics of the wildfire, but also to the measurement techniques and models used to study all the properties.

4.5.2. Radiative forcing of aerosols from biomass burning

As mentioned above through the b_{scat} study, the absorption properties of the aerosols vary during the fire event as shown by the SSA values (Table 6). On the first day (18 August) SSA values are the highest showing the scattering property of the aerosols studied. In the following days as fire smoke arrived, the SSA values decrease for a given wavelength, meaning that aerosols are more absorbing in that wavelength. Consequently, a warming of the atmosphere occurs, as shown in Table 7, with positive direct radiative forcing.

The GAME simulations were performed with data from 18 to 21 August to study the evolution of atmospheric, surface and top of the atmosphere radiative forcing with the incoming of biomass burning plumes.

The instantaneous surface radiative forcing can reach up to −137.4 W m^{-2} on 21 August at 1000 UTC. The corresponding daytime average is −128.3 ± 9.2 W m^{-2} for mean AOD of 0.38 and calculated refractive index of 1.576–0.048*i*. The attenuation of the incoming solar flux is high in response to the high loading of biomass burning aerosols in the atmosphere with important extinction (high scattering and absorbing) properties.

Instantaneous ΔFTOA vary between −14 W m^{-2} and −1.8 W m^{-2} all along the studied days. The daytime average of radiative forcing at TOA vary between −10.1 ± 3.1 W m^{-2} and −4.4 ± 3.1 W m^{-2}. The surface cooling does not balance the TOA aerosol radiative forcing, meaning that aerosols exert a positive net atmospheric forcing due to their ability to absorb solar radiation. Moreover, compared to values found in the literature, our daytime average of the radiative forcing is

Table 4
Coefficients of scattering (b_{scat}), absorption (b_{abs}), extinction (b_{ext}) and backscattering (b_{bscat}) for the total aerosol size distribution, fine mode and coarse mode in three wavelengths (440, 670 and 870 nm) on 18, 19, 20, 21 and 22 August 2012. The days in which León was affected by the forest fire plumes have been highlighted in bold.

Wavelength	Daytime (07:00–19:00 UTC)	Total distribution of aerosols				Fine mode				Coarse mode			
		b_{scat} (Mm^{-1})	b_{abs} (Mm^{-1})	b_{ext} (Mm^{-1})	b_{bscat} (Mm^{-1})	b_{scat} (Mm^{-1})	b_{abs} (Mm^{-1})	b_{ext} (Mm^{-1})	b_{bscat} (Mm^{-1})	b_{scat} (Mm^{-1})	b_{abs} (Mm^{-1})	b_{ext} (Mm^{-1})	b_{bscat} (Mm^{-1})
440 nm	18/08/2012	21.7 ± 4.7	8.4 ± 2.4	30.1 ± 6.6	0.5 ± 0.1	14.0 ± 4.4	2.5 ± 0.7	16.6 ± 5.2	0.4 ± 0.1	7.7 ± 3.2	5.9 ± 2.4	13.5 ± 5.6	0.1 ± 0.0
	19/08/2012	**14.9 ± 5.8**	**7.4 ± 3.3**	**22.2 ± 9.1**	**0.2 ± 0.1**	**10.0 ± 3.4**	**3.1 ± 1.1**	**13.1 ± 4.5**	**0.2 ± 0.1**	**4.9 ± 2.5**	**4.2 ± 2.2**	**9.1 ± 4.7**	**0.0 ± 0.0**
	20/08/2012	**27.7 ± 11.5**	**13.5 ± 6.3**	**41.2 ± 17.7**	**0.5 ± 0.2**	**18.8 ± 7.0**	**5.9 ± 2.1**	**24.7 ± 9.1**	**0.4 ± 0.1**	**8.9 ± 5.4**	**7.6 ± 4.6**	**16.6 ± 9.9**	**0.0 ± 0.0**
	21/08/2012	**49.8 ± 39.4**	**20.8 ± 13.6**	**70.6 ± 52.9**	**0.7 ± 0.4**	**37.8 ± 33.2**	**10.6 ± 8.2**	**48.4 ± 41.4**	**0.6 ± 0.4**	**11.9 ± 6.4**	**10.3 ± 5.5**	**22.2 ± 12.0**	**0.1 ± 0.0**
	22/08/2012	35.7 ± 7.5	10.6 ± 2.3	46.3 ± 9.0	0.6 ± 0.1	27.1 ± 7.6	4.1 ± 1.0	31.2 ± 8.6	0.5 ± 0.1	8.6 ± 2.7	6.5 ± 2.1	15.1 ± 4.9	0.1 ± 0.0
670 nm	18/08/2012	13.5 ± 3.6	7.0 ± 2.3	20.5 ± 5.9	0.4 ± 0.1	5.1 ± 1.4	1.4 ± 0.4	6.5 ± 1.8	0.2 ± 0.1	8.4 ± 3.5	5.6 ± 2.4	14.0 ± 5.8	0.2 ± 0.1
	19/08/2012	**8.7 ± 3.6**	**6.0 ± 2.8**	**14.7 ± 6.4**	**0.2 ± 0.1**	**3.7 ± 1.1**	**1.7 ± 0.6**	**5.4 ± 1.7**	**0.1 ± 0.1**	**5.0 ± 2.6**	**4.3 ± 2.2**	**9.3 ± 4.8**	**0.0 ± 0.0**
	20/08/2012	**15.9 ± 7.6**	**11.0 ± 5.6**	**26.9 ± 13.1**	**0.3 ± 0.1**	**6.8 ± 2.6**	**3.2 ± 1.1**	**10.0 ± 3.7**	**0.3 ± 0.1**	**9.1 ± 5.5**	**7.8 ± 4.7**	**16.9 ± 10.2**	**0.1 ± 0.0**
	21/08/2012	**27.6 ± 21.8**	**16.3 ± 10.1**	**43.8 ± 31.9**	**0.6 ± 0.5**	**15.3 ± 15.4**	**5.8 ± 4.6**	**21.1 ± 20.0**	**0.5 ± 0.4**	**12.3 ± 6.7**	**10.4 ± 5.6**	**22.7 ± 12.2**	**0.1 ± 0.1**
	22/08/2012	20.7 ± 3.9	8.5 ± 2.1	29.2 ± 5.6	0.5 ± 0.1	11.3 ± 3.4	2.2 ± 0.6	13.5 ± 4.0	0.3 ± 0.1	9.4 ± 3.0	6.3 ± 2.1	15.6 ± 5.0	0.2 ± 0.0
870 nm	18/08/2012	11.8 ± 4.0	6.4 ± 2.2	18.3 ± 6.2	0.4 ± 0.1	2.6 ± 0.6	1.0 ± 0.3	3.6 ± 0.9	0.1 ± 0.0	9.2 ± 3.8	5.4 ± 2.3	14.7 ± 6.1	0.3 ± 0.1
	19/08/2012	**7.2 ± 3.2**	**5.5 ± 2.7**	**12.7 ± 5.9**	**0.2 ± 0.1**	**1.9 ± 0.6**	**1.2 ± 0.4**	**3.1 ± 1.0**	**0.1 ± 0.0**	**5.3 ± 2.7**	**4.3 ± 2.2**	**9.6 ± 4.9**	**0.1 ± 0.0**
	20/08/2012	**13.0 ± 6.7**	**10.1 ± 5.4**	**23.1 ± 12.0**	**0.3 ± 0.1**	**3.5 ± 1.4**	**2.2 ± 0.8**	**5.7 ± 2.1**	**0.2 ± 0.1**	**9.5 ± 5.6**	**7.9 ± 4.7**	**17.4 ± 10.4**	**0.1 ± 0.1**
	21/08/2012	**21.1 ± 15.7**	**14.5 ± 8.7**	**35.6 ± 24.4**	**0.5 ± 0.4**	**8.2 ± 8.7**	**4.0 ± 3.2**	**12.3 ± 11.9**	**0.3 ± 0.3**	**12.9 ± 7.2**	**10.5 ± 5.5**	**23.4 ± 12.7**	**0.2 ± 0.2**
	22/08/2012	16.3 ± 3.2	7.6 ± 2.0	23.9 ± 5.1	0.5 ± 0.1	6.0 ± 1.8	1.5 ± 0.4	7.5 ± 2.2	0.2 ± 0.1	10.3 ± 3.2	6.1 ± 2.0	16.4 ± 5.2	0.3 ± 0.1

Table 5
Mass scattering efficiency scattering efficiency (*MSE*), mass absorption efficiency (*MAE*), mass extinction efficiency (*MEE*) and mass backscattering efficiency (*MBSE*) for the total aerosol size distribution, fine mode and coarse mode in three wavelengths (440, 670 and 870 nm) on 18, 19, 20, 21 and 22 August 2012. The days in which León was affected by the forest fire plumes have been highlighted in bold.

Wavelength	Daytime (07:00–19:00 UTC)	Total distribution of aerosols				Fine mode				Coarse mode			
		MSE ($m^2\ g^{-1}$)	MAE ($m^2\ g^{-1}$)	MEE ($m^2\ g^{-1}$)	MBSE ($m^2\ g^{-1}$)	MSE ($m^2\ g^{-1}$)	MAE ($m^2\ g^{-1}$)	MEE ($m^2\ g^{-1}$)	MBSE ($m^2\ g^{-1}$)	MSE ($m^2\ g^{-1}$)	MAE ($m^2\ g^{-1}$)	MEE ($m^2\ g^{-1}$)	MBSE ($m^2\ g^{-1}$)
440 nm	18/08/2012	0.41 ± 0.16	0.15 ± 0.03	0.55 ± 0.19	0.01 ± 0.00	2.65 ± 0.16	0.48 ± 0.01	3.12 ± 0.17	0.07 ± 0.00	0.15 ± 0.03	0.11 ± 0.02	0.26 ± 0.04	0.00 ± 0.00
	19/08/2012	**0.65 ± 0.13**	**0.32 ± 0.06**	**0.97 ± 0.18**	**0.01 ± 0.00**	**4.34 ± 0.22**	**1.36 ± 0.02**	**5.71 ± 0.25**	**0.10 ± 0.00**	**0.23 ± 0.04**	**0.20 ± 0.04**	**0.43 ± 0.08**	**0.00 ± 0.00**
	20/08/2012	**0.62 ± 0.18**	**0.29 ± 0.07**	**0.91 ± 0.25**	**0.01 ± 0.00**	**4.38 ± 0.25**	**1.37 ± 0.03**	**5.75 ± 0.28**	**0.10 ± 0.00**	**0.20 ± 0.04**	**0.17 ± 0.03**	**0.38 ± 0.07**	**0.00 ± 0.00**
	21/08/2012	**0.67 ± 0.20**	**0.29 ± 0.06**	**0.96 ± 0.26**	**0.01 ± 0.00**	**4.89 ± 0.57**	**1.42 ± 0.06**	**6.32 ± 0.63**	**0.09 ± 0.01**	**0.19 ± 0.02**	**0.16 ± 0.02**	**0.35 ± 0.04**	**0.00 ± 0.00**
	22/08/2012	0.60 ± 0.32	0.17 ± 0.04	0.77 ± 0.37	0.01 ± 0.01	3.52 ± 0.34	0.53 ± 0.02	4.04 ± 0.36	0.07 ± 0.00	0.15 ± 0.03	0.11 ± 0.02	0.26 ± 0.04	0.00 ± 0.00
670 nm	18/08/2012	0.24 ± 0.06	0.12 ± 0.02	0.36 ± 0.07	0.01 ± 0.00	0.97 ± 0.10	0.26 ± 0.01	1.24 ± 0.10	0.04 ± 0.00	0.16 ± 0.03	0.11 ± 0.02	0.26 ± 0.04	0.00 ± 0.00
	19/08/2012	**0.38 ± 0.07**	**0.26 ± 0.04**	**0.64 ± 0.11**	**0.01 ± 0.00**	**1.62 ± 0.13**	**0.75 ± 0.01**	**2.37 ± 0.14**	**0.06 ± 0.00**	**0.24 ± 0.04**	**0.20 ± 0.04**	**0.44 ± 0.08**	**0.00 ± 0.00**
	20/08/2012	**0.34 ± 0.08**	**0.23 ± 0.05**	**0.58 ± 0.12**	**0.01 ± 0.00**	**1.58 ± 0.13**	**0.75 ± 0.01**	**2.33 ± 0.15**	**0.06 ± 0.00**	**0.21 ± 0.04**	**0.18 ± 0.03**	**0.39 ± 0.07**	**0.00 ± 0.00**
	21/08/2012	**0.37 ± 0.10**	**0.23 ± 0.04**	**0.60 ± 0.14**	**0.01 ± 0.00**	**1.89 ± 0.38**	**0.78 ± 0.04**	**2.67 ± 0.42**	**0.07 ± 0.00**	**0.19 ± 0.02**	**0.17 ± 0.02**	**0.36 ± 0.04**	**0.00 ± 0.00**
	22/08/2012	0.34 ± 0.14	0.13 ± 0.02	0.47 ± 0.17	0.01 ± 0.00	1.46 ± 0.20	0.29 ± 0.01	1.76 ± 0.22	0.04 ± 0.00	0.16 ± 0.03	0.11 ± 0.02	0.27 ± 0.04	0.00 ± 0.00
870 nm	18/08/2012	0.21 ± 0.04	0.11 ± 0.01	0.32 ± 0.05	0.01 ± 0.00	0.51 ± 0.07	0.18 ± 0.00	0.69 ± 0.08	0.02 ± 0.00	0.17 ± 0.03	0.10 ± 0.01	0.28 ± 0.05	0.01 ± 0.00
	19/08/2012	**0.31 ± 0.05**	**0.24 ± 0.04**	**0.54 ± 0.09**	**0.01 ± 0.00**	**0.84 ± 0.07**	**0.53 ± 0.01**	**1.37 ± 0.08**	**0.04 ± 0.00**	**0.25 ± 0.04**	**0.20 ± 0.04**	**0.45 ± 0.08**	**0.00 ± 0.00**
	20/08/2012	**0.28 ± 0.05**	**0.21 ± 0.04**	**0.49 ± 0.09**	**0.01 ± 0.00**	**0.81 ± 0.08**	**0.52 ± 0.01**	**1.33 ± 0.09**	**0.04 ± 0.00**	**0.22 ± 0.04**	**0.18 ± 0.03**	**0.40 ± 0.07**	**0.00 ± 0.00**
	21/08/2012	**0.29 ± 0.07**	**0.20 ± 0.03**	**0.49 ± 0.09**	**0.01 ± 0.00**	**0.99 ± 0.24**	**0.55 ± 0.03**	**1.54 ± 0.26**	**0.04 ± 0.00**	**0.20 ± 0.03**	**0.17 ± 0.02**	**0.37 ± 0.04**	**0.00 ± 0.00**
	22/08/2012	0.26 ± 0.08	0.12 ± 0.02	0.38 ± 0.10	0.01 ± 0.00	0.77 ± 0.12	0.20 ± 0.01	0.97 ± 0.12	0.03 ± 0.00	0.18 ± 0.04	0.10 ± 0.01	0.29 ± 0.05	0.01 ± 0.00

Table 6
Input parameters for GAME model: Single Scattering Albedo (SSA) and asymmetry parameter (g) from 18 to 21 August 2012 at 0700, 1000, 1300 and 1600 UTC for 400 nm, 550 nm and 850 nm wavelengths. AOD values are instantaneous AERONET data (440 nm) except the * one, which is the only mean available at this date. The days in which León was affected by the forest fire plumes have been highlighted in bold.

AOD	Date (day/hours (UTC))		Optical properties					
			SSA			g		
			Wavelengths (E.E.A. (European Environment Agency))			Wavelengths (E.E.A. (European Environment Agency))		
			400	550	850	400	550	850
0,27*	18/08/2012	0700	0,86	0,84	0,76	0,73	0,68	0,60
	18/08/2012	1000	0,85	0,82	0,74	0,72	0,67	0,60
	18/08/2012	1300	0,83	0,80	0,73	0,73	0,70	0,66
	18/08/2012	1600	0,79	0,75	0,67	0,74	0,72	0,71
0,43	**19/08/2012**	**0700**	**0,75**	**0,76**	**0,73**	**0,73**	**0,71**	**0,67**
0,40	**19/08/2012**	**1000**	**0,75**	**0,75**	**0,72**	**0,73**	**0,71**	**0,69**
0,37	**19/08/2012**	**1300**	**0,76**	**0,76**	**0,73**	**0,73**	**0,70**	**0,67**
0,25	**19/08/2012**	**1600**	**0,77**	**0,77**	**0,74**	**0,70**	**0,68**	**0,64**
0,40	**20/08/2012**	**0700**	**0,75**	**0,77**	**0,75**	**0,73**	**0,71**	**0,67**
0,41	**20/08/2012**	**1000**	**0,75**	**0,75**	**0,72**	**0,73**	**0,71**	**0,68**
0,37	**20/08/2012**	**1300**	**0,77**	**0,78**	**0,77**	**0,72**	**0,70**	**0,65**
0,35	**20/08/2012**	**1600**	**0,78**	**0,79**	**0,78**	**0,72**	**0,69**	**0,64**
0,10	**21/08/2012**	**0700**	**0,77**	**0,77**	**0,75**	**0,72**	**0,70**	**0,66**
0,13	**21/08/2012**	**1000**	**0,77**	**0,78**	**0,75**	**0,72**	**0,70**	**0,66**
0,10	**21/08/2012**	**1300**	**0,74**	**0,77**	**0,78**	**0,74**	**0,73**	**0,68**
0,08	**21/08/2012**	**1600**	**0,76**	**0,78**	**0,78**	**0,73**	**0,71**	**0,67**

of the same order of magnitude but higher during the fire events due to the high absorbing property of the refractive index. Indeed, Formenti et al. (2002), from the STAAARTE MED 1998 experiment, for AOD of about 0.3, for refractive index of 1.55–0.025i, estimated daytime average TOA radiative forcing of -12 ± 5 W m^{-2} over sea plus vegetation surface. Fiebig et al. (2003) found solar radiative forcing at the tropopause of the same order as our simulations by considering forest fire aerosols in internal mixture near the source with aging by coagulation.

Positive instantaneous ΔFATM forcing given by GAME indicates the absorption of solar radiation in the atmosphere by the smoke aerosols. It varies between $+58.3$ W m^{-2} and $+134.6$ W m^{-2} reaching the peaks when smoke aerosols are the most concentrated (AOD = 0.43). In Table 7, the daytime average atmospheric radiative forcing is the highest (on 19 and 20 August) when aerosol loading is high (the highest AODs), while concentrations of fine aerosols are important and the refractive index is representative of specific burnt species.

4.6. Inhalable, thoracic, tracheobronchial and respirable fractions

In addition to the consequences of the fire on radiative forcing, the effects on the population of the city have also been studied. It should be noted that the city of León plus the adjacent municipalities constitute a conurbation with a population of >150,000 inhabitants.

The different mass fractions of aerosol in the city of León were evaluated taking into account the estimated density of the particles, the aerodynamic diameters of the channels of the spectrometer, and the number of particles in each channel during the study period. The calculations were made on the basis of the numerical approximations to the log-normal cumulative distributions, in accordance with the procedure set out in Annex B to the Spanish Standard UNE 77213 (equivalent to International Standard ISO 7708 (1995)). The results are shown in Table 8.

Table 7
Daytime average of direct radiative forcing (W m^{-2}) from 18 to 21 August 2012. The days in which León was affected by the forest fire plumes have been highlighted in bold.

DATE	ΔFBOA	ΔFTOA	ΔFATM
18/08/2012	-85.8 ± 13.4	-10.1 ± 3.1	75.8 ± 14.0
19/08/2012	**-122.0 ± 19.6**	**-4.4 ± 3.1**	**117.6 ± 22.6**
20/08/2012	**-128.3 ± 9.2**	**-5.4 ± 2.6**	**122.9 ± 11.8**
21/08/2012	**-69.5 ± 4.3**	**-9.5 ± 2.2**	**60.0 ± 2.7**

The smoke plumes caused changes in aerosol size distributions, and consequently also in the mass retained in the different parts of the respiratory tract. The population was exposed to high levels of pollution caused by the plume of smoke over the city, with very high levels at certain time intervals. It has been estimated that healthy adults might have retained up to 47 μg m^{-3} (episode average of 16 μg m^{-3}) in the trachea and bronchia (tracheobronchial region), and up to 43 μg m^{-3} reach the bronchioles and alveoli (alveolar region) (episode average of 11 μg m^{-3}). People at high risk like children, frail and sick people might have retained up to 54 μg m^{-3} in the tracheobronchial region (episode average of 19 μg m^{-3}) and 29 μg m^{-3} in the alveolar region (episode average of 7 μg m^{-3}).

5. Conclusions

In this paper, a strong subsidence thermal inversion that induced changes on the dispersion and medium range transport of the smoke plumes from two forest fires has been studied. Under this situation, the plumes arrived in a city (León, Spain) at around 70 km from the fires, with large amounts of ashes.

Air quality was dramatically altered as the smoke plumes arrived in the city, with considerable increases of PM_{10} and $PM_{2.5}$, confirmed by a simultaneous increase in gas concentrations. An increase in the concentration of particles in the fine mode, especially particles smaller than 0.2 μm was recorded. Then, a gradual increase of the median size from 0.09 to 0.14 μm was also found during the pollution event, probably due to oxidation undergone by the aerosols during their stay in the atmosphere. Concerning to this point, one of the main contributions that this study can provide is the recommendation to study the aging of the aerosol from fires, mainly in relation with health and radiative forcing, as explained below.

The plumes arrival caused an increase in the radiation absorption processes. The radiative atmospheric forcing detected, as well as the consequent solar dimming at the surface, may largely impact the dynamic, thermodynamic and photochemical properties of the atmospheric boundary layer, at the same time deteriorating the air quality.

Since the wildfires in the northwest of Iberia are more and more frequent in recent years, this estimate of warming is becoming essential. The fires are probably generating deep alterations in regional atmospheric stability because they vary not only surface temperatures (hence altering heating rates), but also rain formation as a consequence

Table 8
Inhalable, thoracic, tracheobronchial and respirable mass fractions for healthy adults and high-risk population (children, frail or sick people) deposited in the respiratory tract, on 19, 20 and 21 August 2012. Mean daily values and hourly values during the hour of maximum PM concentration.

Day	Inhalable fraction ($\mu g\ m^{-3}$)	Thoracic fraction ($\mu g\ m^{-3}$)	Tracheobronchial fraction-healthy adult ($\mu g\ m^{-3}$)	Tracheobronchial fraction-high risk ($\mu g\ m^{-3}$)	Respirable fraction-healthy adult ($\mu g\ m^{-3}$)	Respirable fraction-high risk ($\mu g\ m^{-3}$)
19/08/2012	26 ± 13	18 ± 9	11 ± 6	14 ± 7	7 ± 3	4 ± 2
20/08/2012	43 ± 31	29 ± 21	18 ± 13	22 ± 16	11 ± 8	7 ± 5
21/08/2012	46 ± 24	31 ± 16	18 ± 9	22 ± 11	14 ± 7	9 ± 5
Maximum of day (hour)						
19/08/2012 (0800 UTC)	47	27	19	22	8	5
20/08/2012 (1900 UTC)	121	63	47	54	16	9
21/08/2012 (1200 UTC)	111	75	32	46	43	29

of changes in regional cloud cover. Therefore, the determination of regional climate feedbacks requires further applications of models at a regional scale for which the parameters from wildfires become essential.

Due to the forest fires studied, the population in León was exposed to important concentrations of fine particles, especially dangerous for human health. It has been estimated that healthy adults might have retained up to 47 $\mu g\ m^{-3}$ in the trachea and bronchia (tracheobronchial region), and up to 43 $\mu g\ m^{-3}$ reached the bronchioles and alveoli (alveolar region).

Although it is well known that emissions from fires represent noteworthy contributions to global mortality rates, the last result suggests a further study about the incidence of wildfires on human health even in populations far away from the location of the fire. For example, the development of new studies addressing morbidity due to respiratory tract diseases during wildfires (even when they occur in remote areas) would be desirable. Furthermore, also concerning human health, not only the size of the particles contained in the smoke plume must be determined. As potentially hazardous emissions coming from forest fire smoke contain carcinogenic compounds such as free radicals, benzene and polycyclic aromatic hydrocarbons (PAHs), it is advisable to evaluate the chemical composition of the air that the local community is breathing, in order to verify that the concentrations do not exceed the limits allowed, even when the fire seems to be far away.

In summary, although it is not easy to find simultaneously the same conditions of the large forest fire that we have studied (with an intense subsidence inversion and a plume trajectory passing over the sampling point), it would be desirable in future studies to analyze the chemical composition of transported aerosols, ultrafine particle distributions (which, from the physical point of view, are the most dangerous for human health due to its great penetration power in the respiratory tract) and the radiative characteristics of the material transported by the smoke plume.

This paper has illustrated the importance of the weather conditions in the dispersion of pollutants. Thus, a strong subsidence inversion associated to a high-pressure system inhibited vertical dispersion with a consequent transport of pollutants to a city far away from the fire sites, that affected the health of the population, visibility and radiative forcing. Most of the studies related to biomass burning aerosols emphasize the uncertainties concerned the aging processes of particles after being emitted. Future field projects should also include continuous measurements of aerosol composition and smoke markers, so that information on the aerosol behavior and evolution can be provided to improve understanding of aerosol dynamical processes of the fire plumes.

Finally, the originality of a work like this about forest fires may be due to the fact that forest fires are events of opportunistic behavior and of relatively short duration, which hampers the establishment of significant conclusions about human health, climate alteration or the dispersion of the products of combustion. In terms of health, we need to better understand the characteristics of smoke both near or far from wildfires and their probable consequences, to adjust the response of the people potentially unprotected from exposure to smoke.

Acknowledgements

This study was partially supported by the Spanish Ministry of Economy and Competitiveness (Grant TEC2014-57821-R), the University of León (Programa Propio 2015/00054/001) and the AERORAIN project (Ministry of Economy and Competitiveness, Grant CGL2014-52556-R, co-financed with FEDER funds). The authors wish to thank the Consejería de Medio Ambiente de la Junta de Castilla y León and the City of León for their assistance whenever needed. The authors gratefully acknowledge Darrel Baumgardner for his help with the code developed by Bohern and Huffman and the optical properties code, and the NOAA Air Resources Laboratory (ARL) for the HYSPLIT transport and dispersion model and/or READY website (http://www.ready.noaa.gov) used in this publication. We also want to thank Victoria Cachorro Revilla for providing the AERONET data in Palencia, and Philippe Dubuisson for the maintenance and development of the GAME model. Noelia Ramón patiently revised the final version in English.

Appendix A. Supplementary data

Supplementary data to this article can be found online at https://doi.org/10.1016/j.scitotenv.2017.11.142.

References

Adler, G., Riziq, A.A., Erlick, C., Rudich, Y., 2010. Effect of intrinsic organic carbon on the optical properties of fresh diesel soot. Proc. Natl. Acad. Sci. 107, 6699–6704.
Adler, G., Flores, J.M., Abo Riziq, A., Borrmann, S., Rudich, Y., 2011. Chemical, physical, and optical evolution of biomass burning aerosols: a case study. Atmos. Chem. Phys. 11, 1491–1503.
Alonso-Blanco, E., Calvo, A.I., Pont, V., Mallet, M., Fraile, R., Castro, A., 2014. Impact of biomass burning on aerosol size distribution, aerosol optical properties and associated radiative forcing. Aerosol Air Qual. Res. 14, 708–724.
Alves, C.A., Gonçalves, C., Pio, C.A., Mirante, F., Caseiro, A., Tarelho, L., Freitas, M.C., Viegas, D.X., 2010. Smoke emissions from biomass burning in a Mediterranean shrubland. Atmos. Environ. 44, 3024–3033.
Alves, C., Calvo, A.I., Marques, L., Castro, A., Nunes, T., Coz, E., Fraile, R., 2014. Particulate matter in the indoor and outdoor air of a gymnasium and a fronton. Environ. Sci. Pollut. Res. 21, 12390–12402 (Doi 12310.11007/s11356-12014-13168-12391).
Amaral, S.S., de Carvalho Junior, J.A., Costa, M.A.M., Neto, T.G.S., Dellani, R., Leite, L.H.S., 2014. Comparative study for hardwood and softwood forest biomass: chemical characterization, combustion phases and gas and particulate matter emissions. Bioresour. Technol. 164, 55–63.
Amiridis, V., Zerefos, C., Kazadzis, S., Gerasopoulos, E., Eleftheratos, K., Vrekoussis, M., Stohl, A., Mamouri, R.E., Kokkalis, P., Papayannis, A., 2012. Impact of the 2009 Attica wild fires on the air quality in urban Athens. Atmos. Environ. 46, 536–544.
Andreae, M.O., Merlet, P., 2001. Emission of trace gases and aerosols from biomass burning. Glob. Biogeochem. Cycles 15, 955–966.
Badarinath, K.V.S., Madhavi Latha, K., Kiran Chand, T.R., Gupta, P.K., Ghosh, A.B., Jain, S.L., Gera, B.S., Singh, R., Sarkar, A.K., Singh, N., 2004. Characterization of aerosols from biomass burning: a case study from Mizoram (Northeast), India. Chemosphere 54, 167–175.

Barnaba, F., Angelini, F., Curci, G., Gobbi, G.P., 2011. An important fingerprint of wildfires on the European aerosol load. Atmos. Chem. Phys. 11, 10487–10501.

Bohren, C.F., Huffman, D.R., 1983. Absorption and Scattering of Light by Small Particles. Wiley, New York.

Calvo, A., Pont, V., Castro, A., Mallet, M., Palencia, C., Roger, J.-C., Dubuisson, P., Fraile, R., 2010. Radiative forcing of haze during a forest fire in Spain. J. Geophys. Res. Atmos. 115.

Calvo, A., Tarelho, L., Teixeira, E., Alves, C., Nunes, T., Duarte, M., Coz, E., Custodio, D., Castro, A., Artinano, B., 2013. Particulate emissions from the co-combustion of forest biomass and sewage sludge in a bubbling fluidised bed reactor. Fuel Process. Technol. 114, 58–68.

Capes, G., Johnson, B., McFiggans, G., Williams, P., Haywood, J., Coe, H., 2008. Aging of biomass burning aerosols over West Africa: aircraft measurements of chemical composition, microphysical properties, and emission ratios. J. Geophys. Res. Atmos. 113.

Carrico, C.M., Kreidenweis, S.M., Malm, W.C., Day, D.E., Lee, T., Carrillo, J., McMeeking, G.R., Collett Jr, J.L., 2005. Hygroscopic growth behavior of a carbon-dominated aerosol in Yosemite National Park. Atmos. Environ. 39, 1393–1404.

Carslaw, K., Boucher, O., Spracklen, D., Mann, G., Rae, J., Woodward, S., Kulmala, M., 2010. A review of natural aerosol interactions and feedbacks within the Earth system. Atmos. Chem. Phys. 10, 1701–1737.

Castro, A., Calvo, A.I., Alves, C., Alonso-Blanco, E., Coz, E., Marques, L., Nunes, T., Fernández-Guisuraga, J.M., Fraile, R., 2015. Indoor aerosol size distributions in a gymnasium. Sci. Total Environ. 524, 178–186.

Cheng, Z., Jiang, J., Chen, C., Gao, J., Wang, S., Watson, J.G., Wang, H., Deng, J., Wang, B., Zhou, M., 2014. Estimation of aerosol mass scattering efficiencies under high mass loading: case study for the megacity of Shanghai, China. Environ. Sci. Technol. 49, 831–838.

Christensen, J.H., 1997. The Danish eulerian hemispheric model: a three-dimensional air pollution model used for the arctic. Atmos. Environ. 31, 4169–4191.

Coz, E., Gómez-Moreno, F.J., Pujadas, M., Casuccio, G.S., Lersch, T.L., Artíñano, B., 2009. Individual particle characteristics of North African dust under different long-range transport scenarios. Atmos. Environ. 43, 1850–1863.

Delmas, R., Lacaux, J.P., Menaut, J.C., Abbadie, L., Le Roux, X., Helas, G., Lobert, J., 1995. Nitrogen compound emission from biomass burning in tropical African savanna FOS/DECAFE 1991 Experiment (Lamto, Ivory Coast). J. Atmos. Chem. 22, 175–193.

Deng, X., Tie, X., Zhou, X., Wu, D., Zhong, L., Tan, H., Li, F., Huang, X., Bi, X., Deng, T., 2008. Effects of Southeast Asia biomass burning on aerosols and ozone concentrations over the Pearl River Delta (PRD) region. Atmos. Environ. 42, 8493–8501.

Dimitriou, K., McGregor, G., Kassomenos, P., Paschalidou, A., 2016. Exploring winter mortality variability in five regions of England, using back trajectory analysis. Earth Interact. 20 (1). https://doi.org/10.1175/EI-D-15-0012.1.

Draxler, R.R., Rolph, G.D., 2013. HYSPLIT (HYbrid Single-Particle Lagrangian Integrated Trajectory) Model access via NOAA ARL READY Website. http://www.arl.noaa.gov/HYSPLIT.php NOAA Air Resources Laboratory, College Park, MD.

Duan, F., Liu, X., Yu, T., Cachier, H., 2004. Identification and estimate of biomass burning contribution to the urban aerosol organic carbon concentrations in Beijing. Atmos. Environ. 38, 1275–1282.

Dubuisson, P., Buriez, J., Fouquart, Y., 1996. High spectral resolution solar radiative transfer in absorbing and scattering media: application to the satellite simulation. J. Quant. Spectrosc. Radiat. Transf. 55, 103–126.

Dubuisson, P., Dessailly, D., Vesperini, M., Frouin, R., 2004. Water vapor retrieval over ocean using near-infrared radiometry. J. Geophys. Res. Atmos. 109.

E.E.A. (European Environment Agency), 1999. Environment in the European Union at the Turn of the Century. Environmental Assessment Report No 2.

Fernández-González, S., del Río, S., Castro, A., Penas, A., Fernández-Raga, M., Calvo, A., Fraile, R., 2012. Connection between NAO, weather types and precipitation in León, Spain (1948–2008). Int. J. Climatol. 32, 2181–2196.

Fiebig, M., Stohl, A., Wendisch, M., Eckhardt, S., Petzold, A., 2003. Dependence of solar radiative forcing of forest fire aerosol on ageing and state of mixture. Atmos. Chem. Phys. 3, 881–891.

Formenti, P., Boucher, O., Reiner, T., Sprung, D., Andreae, M.O., Wendisch, M., Wex, H., Kindred, D., Tzortziou, M., Vasaras, A., 2002. STAAARTE-MED 1998 summer airborne measurements over the Aegean Sea 2. Aerosol scattering and absorption, and radiative calculations. J. Geophys. Res. Atmos. 107.

Forster, P., Ramaswamy, V., Artaxo, P., Berntsen, T., Betts, R., Fahey, D.W., Haywood, J., Lean, J., Lowe, D.C., Myhre, G., Nganga, J., Prinn, R., Raga, G., Schulz, M., Van Dorland, R., 2007. Changes in atmospheric constituents and in radiative forcing. In: Solomon, S., Qin, D., Manning, M., Chen, Z., Marquis, M., Averyt, K.B., Tignor, M., Miller, H.L. (Eds.), Climate Change 2007: The Physical Science Basis. Contribution of Working Group I to the Fourth Assessment Report of the Intergovernmental Panel on Climate Change. Cambridge University Press, Cambridge, United Kingdom and New York, NY, USA.

Goodess, C., Jones, P., 2002. Links between circulation and changes in the characteristics of Iberian rainfall. Int. J. Climatol. 22, 1593–1615.

Hansell Jr, R.A., Reid, J.S., Tsay, S.C., Roush, T.L., Kalashnikova, O.V., 2011. A sensitivity study on the effects of particle chemistry, asphericity and size on the mass extinction efficiency of mineral dust in the earth's atmosphere: from the near to thermal IR. Atmos. Chem. Phys. 11, 1527–1547.

Hasan, H., Dzubay, T., 1983. Apportioning light extinction coefficients to chemical species in atmospheric aerosol. Atmos. Environ. 17, 1573–1581 (1967).

Hess, M., Koepke, P., Schult, I., 1998. Optical properties of aerosols and clouds: the software package OPAC. Bull. Am. Meteorol. Soc. 79, 831–844.

Hsiao, T.-C., Ye, W.-C., Wang, S.-H., Tsay, S.-C., Chen, W.-N., Lin, N.-H., Lee, C.-T., Hung, H.-M., Chuang, M.-T., Chantara, S., 2016. Investigation of the CCN activity, BC and UVBC mass concentrations of biomass burning aerosols during the 2013 BASELInE campaign. Aerosol Air Qual. Res. 16, 2742–2756.

Hungershoefer, K., Zeromskiene, K., Iinuma, Y., Helas, G., Trentmann, J., Trautmann, T., Parmar, R.S., Wiedensohler, A., Andreae, M.O., Schmid, O., 2008. Modelling the optical properties of fresh biomass burning aerosol produced in a smoke chamber: results from the EFEU campaign. Atmos. Chem. Phys. 8, 3427–3439.

IPCC, 2001. Climate Change 2001: Contribution of Working Group I to the Third Assessment Report of the Intergovernmental Panel on Climate Change. Cambridge University Press, Cambridge, United Kingdom and New York, NY, USA.

IPCC, 2013. Climate Change 2013: The Physical Science Basis. Contribution of Working Group I to the Fifth Assessment Report of the Intergovernmental Panel on Climate Change. Cambridge University Press, Cambridge, United Kingdom and New York, NY, USA.

ISO, 1995. International Organization for Standadization (ISO), 1995. ISO 7708:1995 (E): Air Quality-particle Size Fraction Definitions for Health Related Sampling. 1st edition. ISO Publications (1995-04-01).

Janhäll, S., Andreae, M.O., Pöschl, U., 2010. Biomass burning aerosol emissions from vegetation fires: particle number and mass emission factors and size distributions. Atmos. Chem. Phys. 10, 1427–1439.

Jenkinson, A.F., Collison, F.P., 1977. An initial climatology of gales over the north sea. Synoptic Climatology Branch Memorándum, 62. Meteorological Office, London.

Jiang, H., Feingold, G., 2006. Effect of aerosol on warm convective clouds: aerosol-cloud-surface flux feedbacks in a new coupled large eddy model. J. Geophys. Res. Atmos. 111.

Jones, P.D., Hulme, M., Briffa, K.R., 1993. A comparison of lamb circulation types with an objective classification scheme. Int. J. Climatol. 13, 655–663.

Jung, J., Lee, H., Kim, Y.J., Liu, X., Zhang, Y., Hu, M., Sugimoto, N., 2009. Optical properties of atmospheric aerosols obtained by in situ and remote measurements during 2006 Campaign of Air Quality Research in Beijing (CAREBeijing-2006). J. Geophys. Res. 114, D00G02.

Kasischke, E.S., Bruhwiler, L.P., 2002. Emissions of carbon dioxide, carbon monoxide, and methane from boreal forest fires in 1998. J. Geophys. Res. Atmos. 107, 2–14 (1984–2012). FFR 2-1-FFR.

Kim, Y.J., Boatman, J.F., 1990. Size calibration corrections for the active scattering aerosol spectrometer probe (ASASP-100X). Aerosol Sci. Technol. 12, 665–672.

Lamb, H.H., Britain, G., 1972. British Isles Weather Types and a Register of the Daily Sequence of Circulation Patterns 1861–1971. HM Stationery Office.

Levin, E.J.T., McMeeking, G.R., Carrico, C.M., Mack, L.E., Kreidenweis, S.M., Wold, C.E., Moosmüller, H., Arnott, W.P., Hao, W.M., Collett, J.L., 2010. Biomass burning smoke aerosol properties measured during Fire Laboratory at Missoula Experiments (FLAME). J. Geophys. Res. D18210 (115), 115.

Levine, J.S., 1996. Biomass Burning and Global Change: Remote Sensing, Modeling and Inventory Development, and Biomass Burning in Africa. MIT Press.

Liu, H., Chang, W.L., Oltmans, S.J., Chan, L.Y., Harris, J.M., 1999. On springtime high ozone events in the lower troposphere from Southeast Asian biomass burning. Atmos. Environ. 33, 2403–2410.

Löndahl, J., Swietlicki, E., Pagels, J., Massling, A., Boman, C., Rissler, J., Blomberg, A., Thomas, S., 2009. Respiratory tract deposition of particles from biomass combustion. J. Phys. Conf. Ser. 151, 012066.

Mauzerall, D.L., Logan, J.A., Jacob, D.J., Anderson, B.E., Blake, D.R., Bradshaw, J.D., Heikes, B., Sachse, G.W., Singh, H., Talbot, B., 1998. Photochemistry in biomass burning plumes and implications for tropospheric ozone over the tropical South Atlantic. J. Geophys. Res. Atmos. 103, 8401–8423 (1984–2012).

Oberdärster, G., Oberdärster, E., Oberdärster, J., 2005. Nanotoxicology: an emerging discipline evolving from studies of ultrafine particles. Environ. Health Perspect. 113.

Okoshi, R., Rasheed, A., Chen Reddy, G., McCrowey, C.J., Curtis, D.B., 2014. Size and mass distributions of ground-level sub-micrometer biomass burning aerosol from small wildfires. Atmos. Environ. 89, 392–402.

O'Neill, N.T., Eck, T.F., Holben, B.N., Smirnov, A., Royer, A., Li, Z., 2002. Optical properties of boreal forest fire smoke derived from Sun photometry. J. Geophys. Res. Atmos. 107, 6–19 (1984–2012). AAC 6-1-AAC.

Papadopoulos, A., Paschalidou, A.K., Kassomenos, P.A., McGregor, G., 2014. On the association between synoptic circulation and wildfires in the Eastern Mediterranean. Theor. Appl. Climatol. 115 (3–4), 483–501.

Pere, J.-C., Mallet, M., Pont, V., Bessagnet, B., 2011. Impact of aerosol direct radiative forcing on the radiative budget, surface heat fluxes, and atmospheric dynamics during the heat wave of summer 2003 over western Europe: a modeling study. J. Geophys. Res. Atmos. 116.

Pitz, M., Cyrys, J., Karg, E., Wiedensohler, A., Wichmann, H.E., Heinrich, J., 2003. Variability of apparent particle density of an urban aerosol. Environ. Sci. Technol. 37, 4336–4342.

Pope, C.A., 2000. Review: epidemiological basis for particulate air pollution health standards. Aerosol Sci. Technol. 32, 4–14.

Reid, J.S., Hobbs, P.V., 1998. Physical and optical properties of young smoke from individual biomass fires in Brazil. J. Geophys. Res. Atmos. 103, 32013–32030 (1984–2012).

Reid, J.S., Hobbs, P.V., Ferek, R.J., Blake, D.R., Martins, J.V., Dunlap, M.R., Liousse, C., 1998. Physical, chemical, and optical properties of regional hazes dominated by smoke in Brazil. J. Geophys. Res. Atmos. 103, 32059–32080 (1984–2012).

Reid, J.S., Eck, T.F., Christopher, S.A., Koppmann, R., Dubovik, O., Eleuterio, D.P., Holben, B.N., Reid, E.A., Zhang, J., 2004. A review of biomass burning emissions part III: intensive optical properties of biomass burning particles. Atmos. Chem. Phys. Discuss. 4, 5201–5260.

Reid, J.S., Koppmann, R., Eck, T.F., Eleuterio, D.P., 2005. A review of biomass burning emissions part II: intensive physical properties of biomass burning particles. Atmos. Chem. Phys. 5, 799–825.

Rissler, J., Swietlicki, E., Zhou, J., Roberts, G., Andreae, M.O., Gatti, L.V., Artaxo, P., 2004. Physical properties of the sub-micrometer aerosol over the Amazon rain forest during the wet-to-dry season transition-comparison of modeled and measured CCN concentrations. Atmos. Chem. Phys. 4, 2119–2143.

Rissler, J., Vestin, A., Swietlicki, E., Fisch, G., Zhou, J., Artaxo, P., Andreae, M.O., 2006. Size distribution and hygroscopic properties of aerosol particles from dry-season biomass burning in Amazonia. Atmos. Chem. Phys. 6, 471–491.

Rolph, G.D., 2013. Real-time Environmental Applications and Display sYstem (READY) Website. http://www.ready.noaa.gov NOAA Air Resources Laboratory, College Park, MD.

Saarikoski, S., Sillanpää, M., Sofiev, M., Timonen, H., Saarnio, K., Teinilä, K., Karppinen, A., Kukkonen, J., Hillamo, R., 2007. Chemical composition of aerosols during a major biomass burning episode over northern Europe in spring 2006: experimental and modelling assessments. Atmos. Environ. 41, 3577–3589.

Salvador, P., 2004. Characterization of Air Pollution Produced By Particles in Suspension in Madrid. Doctoral Thesis. Faculty of Physics, University Complutense of Madrid, Madrid (Spain).

Schkolnik, G., Chand, D., Hoffer, A., Andreae, M., Erlick, C., Swietlicki, E., Rudich, Y., 2007. Constraining the density and complex refractive index of elemental and organic carbon in biomass burning aerosol using optical and chemical measurements. Atmos. Environ. 41, 1107–1118.

Scholes, R.J., Ward, D.E., Justice, C.O., 1996. Emissions of trace gases and aerosol particles due to vegetation burning in southern hemisphere Africa. J. Geophys. Res. Atmos. 101, 23677–23682 (1984–2012).

Seinfeld, J.H., Pandis, S.N., 2012. Atmospheric Chemistry and Physics: From Air Pollution to Climate Change. John Wiley & Sons.

Sinha, P., Hobbs, P.V., Yokelson, R.J., Bertschi, I.T., Blake, D.R., Simpson, I.J., Gao, S., Kirchstetter, T.W., Novakov, T., 2003. Emissions of trace gases and particles from savanna fires in southern Africa. J. Geophys. Res. Atmos. 108, 8487.

Stamnes, K., Tsay, S.-C., Wiscombe, W., Jayaweera, K., 1988. Numerically stable algorithm for discrete-ordinate-method radiative transfer in multiple scattering and emitting layered media. Appl. Opt. 27, 2502–2509.

Toll, V., Reis, K., Ots, R., Kaasik, M., Männik, A., Prank, M., Sofiev, M., 2015. SILAM and MACC reanalysis aerosol data used for simulating the aerosol direct radiative effect with the NWP model HARMONIE for summer 2010 wildfire case in Russia. Atmos. Environ. 121, 75–85.

UNE 77213:1997, Air quality. Particle Size Fraction Definitions for Health-related Sampling n.d.

Wardoyo, A.Y., Morawska, L., Ristovski, Z.D., Jamriska, M., Carr, S., Johnson, G., 2007. Size distribution of particles emitted from grass fires in the Northern Territory, Australia. Atmos. Environ. 41, 8609–8619.

Wilcox, E., 2010. Stratocumulus cloud thickening beneath layers of absorbing smoke aerosol. Atmos. Chem. Phys. 10, 11769–11777.

Yamasoe, M.A., Artaxo, P., Miguel, A.H., Allen, A.G., 2000. Chemical composition of aerosol particles from direct emissions of vegetation fires in the Amazon Basin: water-soluble species and trace elements. Atmos. Environ. 34, 1641–1653.